UTAP: University of Tokyo, Theoretical Astrophysics
RESCEU: Research Center for the Early Universe

UTAP-236/96
RESCEU-23/96

Strong Gravitational Lensing and Velocity Function as Tools to Probe Cosmological Parameters: Current Constraints and Future Predictions

Takahiro T. NAKAMURA[1*)] and Yasushi SUTO[1,2**)]

[1] *Department of Physics, University of Tokyo, Tokyo, 113, Japan*
[2] *Research Center for the Early Universe, University of Tokyo, Tokyo, 113, Japan*

Constraints on cosmological models from strong gravitational lensing statistics are investigated. We pay particular attention to the role of the velocity function in the calculation of the lensing probability. The velocity function derived from the observed galaxy luminosity function, which is used in most previous work, is unable to predict the large separation lensing events. In this paper, we also use the Press-Schechter theory to construct a velocity function theoretically. Model predictions are compared with the observed velocity function and the HST snapshot survey. Comparison with the latter observation shows that the predictions based on the theoretical velocity function are consistent with the observed large separation events in COBE normalized low-density models, especially with a non-vanishing cosmological constant. Adopting the COBE normalization, however, we could find no model which simultaneously satisfies both the observed velocity function and the HST snapshot survey. We systematically investigate various uncertainties in the gravitational lensing statistics including finite core radius, the distance formula, magnification bias, and dust obscuration. The results are very sensitive to these effects as well as theoretical models for the velocity function, implying that current limits on the cosmological parameters should be interpreted with caution. Predictions for future surveys are also presented.

§1. Introduction

To date, it is well known that the probability of gravitational lensing (hereafter GL) of high redshift objects is sensitive to the cosmological constant Λ through the geometrical effect [1), 2), 3), 4)] and that extremely Λ-dominated universes predict too many lensing events which is inconsistent with the observed low frequency of lensed quasars in current samples [5), 6), 7)]. Kochanek [8)], for example, concludes that $\lambda_0 := \Lambda/(3H_0^2) < 0.66$ at 95% confidence.

GL limits on λ_0 should be contrasted to the other cosmological tests which favor low density universes with non-vanishing λ_0. The latter tests include the two point angular correlation function of galaxies [9)], the galaxy number counts [10)], the cluster mass and peculiar velocity functions [11), 13), 12), 14)] (See Refs. [15), 16)] for reviews). Moreover, the recent measurements of the (local) Hubble constant $H_0 =: 100h\,\mathrm{km\,s^{-1}Mpc^{-1}}$ give somewhat large values around $h \sim 0.7$–0.8 [17), 18), 19), 20)]. To reconcile the age of the universe $\sim H_0^{-1}$ with that of the oldest globular clusters [21)] and of the young galaxies [22)], it seems inevitable to introduce non-null Λ of $\lambda_0 \gtrsim 0.8$ [23)]. Therefore it is worthwhile reexamining the previous constraints on Λ from GL statistics by taking account of several uncertainties involved in the calculation of GL probability.

In this paper, we pay particular attention to the role of the velocity function (hereafter VF) of lensing objects. Previous work on GL statistics usually uses VF determined from the observed galaxy luminosity function. Moreover, it is often assumed that the comoving number density of lensing objects is constant. However, the luminosity function counts only luminous objects while invisible dark objects might as well be responsible for GL. Bearing this in mind, we also use the VF derived from the Press-Schechter theory [24)] (hereafter PS) with some specific cosmological models such as the

*) E-mail: nakamura@utaphp2.phys.s.u-tokyo.ac.jp
**) E-mail: suto@phys.s.u-tokyo.ac.jp

cold dark matter (CDM) and the primeval isocurvature baryon (PIB) models [25]. The theoretical velocity function, by its construction, properly counts all gravitationally bound dark halos as well as luminous objects, and automatically takes account of the hierarchical evolution of objects for various cosmological parameters [26]. Narayan & White [27] first applied the PS theory to GL statistics, but only in the standard CDM cosmology with no comparison with observation. Kochanek [28] extended their calculation for various cosmological parameters, and argued the constraints on the bias parameter b within the standard CDM model. However, we will see that the PS theory in its original form is not a perfect one in deriving VF, and adopt theoretical attempts towards more realistic VF. We compare these theoretical VF and their predictions on GL statistics with the observed VF [29] and the *HST snapshot survey* [30] for COBE normalized CDM and PIB models.

We also make quantitative estimates of following uncertainties in GL statistics: the effect of inhomogeneity of the universe in the distance formula, the finite core size of lensing objects, the obscuration of images by dusts in the lensing galaxies, and the different definitions of the magnification bias. Although each topic is already discussed separately [6),8),31),32),33),34),35)], we take account of all the above effects consistently and systematically for the first time.

This paper is organized as follows. In §2, we briefly summarize the basic formulae of GL statistics. In §3 we present the VF's which are applied to GL statistics in the later sections. In §4, we compare the theoretical VF and its GL prediction with observation. In §5, we survey various uncertainties described above and see how the results in §4 are affected by them. In §6, we give predictions for future GL surveys. Finally in §7, we summarize the main results of this paper. Our main results are discussed after §4 and are summarized in Table II. Those who are familiar with GL and the PS theory can skip §2 and §3 which are written only for completeness and terminology.

Throughout the paper, we use the units $c = G = 1$. The cosmological parameters are defined as

$$\Omega := \frac{8\pi\bar{\rho}}{3H^2}, \quad \lambda := \frac{\Lambda}{3H^2}, \quad \Omega_0 := \frac{8\pi\bar{\rho}_0}{3H_0^2}, \quad \lambda_0 := \frac{\Lambda}{3H_0^2}, \tag{1·1}$$

$$H := \frac{\dot{a}}{a} = H_0[\Omega_0 a^{-3} + (1-\Omega_0-\lambda_0)a^{-2} + \lambda_0]^{1/2}, \tag{1·2}$$

where $\bar{\rho} = \bar{\rho}_0/a^3 = \bar{\rho}_0(1+z)^3$ is the mean density of the universe at redshift z and the subscripts 0 mean the present epoch $z = 0$.

This paper is largely based on Ref. [36] (unpublished) which contains further detailed discussion.

§2. Brief summary of GL statistics

2.1. *Lens model and GL cross section*

We assume that the lensing objects are spherical and isothermal in describing GL statistics. The spherical lens model gives sufficiently accurate description of the properties of lensed images such as the image separation and the magnification, as compared with more realistic elliptical lens models [37),38),39)]. The isothermal profile is characterized by the internal one-dimensional velocity dispersion v [40]. Thereby we start from the lens potential [41] (twice the Newtonian potential integrated along line-of-sight):

$$\hat{\psi}(\xi) = 4\pi v^2(\xi^2 + \xi_c^2)^{1/2}, \tag{2·1}$$

where ξ is the impact parameter in the lens plane and the core radius ξ_c eliminates the central singularity.*) The lens model with $\xi_c = 0$ is the "singular isothermal sphere" (SIS). Due to the spherical symmetry, the lens equation [41] becomes a scalar equation:

$$\eta = \frac{D_{OS}}{D_{OL}}\xi - D_{LS}\hat{\alpha}(\xi), \tag{2·2}$$

*) The parameter ξ_c defined here approximately corresponds to twice the core radius of Ref. [32].

where η is the source position in the source plane, $D_{\rm OL}$, $D_{\rm OS}$ and $D_{\rm LS}$ are the angular diameter distances between the observer, lens and source, and $\hat{\alpha}(\xi) := (d/d\xi)\hat{\psi}(\xi)$ is the deflection angle. The thin lens approximation, which is implicit in Eq.(2·2), can be justified [42),43),44)] in the case of strong GL, because highly virialized and compact galaxies or clusters are considered here as the lensing objects. Defining

$$\xi_* := 4\pi v^2 \frac{D_{\rm OL} D_{\rm LS}}{D_{\rm OS}}, \quad \eta_* := 4\pi v^2 D_{\rm LS}, \tag{2·3}$$

$$x := \xi/\xi_*\,, \quad y := \eta/\eta_*\,, \quad x_{\rm c} := \xi_{\rm c}/\xi_*\,, \tag{2·4}$$

one can rewrite Eq.(2·2) as

$$y = x - x(x^2 + x_{\rm c}^2)^{-1/2}. \tag{2·5}$$

Given a source position y, the image position x is obtained by solving Eq.(2·5). If $x_{\rm c} < 1$ and $y < y_{\rm r} := (1 - x_{\rm c}^{2/3})^{3/2}\Theta(1 - x_{\rm c})$, triple images form [$\Theta(x)$ is the step function]. The brightness of an image at x is magnified by a factor [41)] $\mu_{\rm p}(x) := |(y/x)(dy/dx)|^{-1}$. When $x_{\rm c} \neq 0$, we solve Eq.(2·5) numerically for the image positions $x_i(y)$ $(i = 1, 2, 3;\ x_1 < x_2 < x_3)$ and calculate $\Delta x(y) := x_3 - x_1$ (separation of the outer two images), $\mu(y) := \sum_i \mu_{\rm p}(x_i)$ (total magnification of all the images), and $r(y) := \exp|\ln[\mu_{\rm p}(x_3)/\mu_{\rm p}(x_1)]|$ (brightness ratio [> 1] of the outer two images). As noted in Ref. [32)], it is safe to approximate $\Delta x(y) \simeq \Delta x(0) = 2x_{\rm t} := 2(1 - x_{\rm c}^2)^{1/2}\Theta(1 - x_{\rm c})$. The separation angle θ in radian is

$$\theta = \frac{2\xi_* x_{\rm t}}{D_{\rm OL}} = 8\pi v^2 \frac{D_{\rm LS}}{D_{\rm OS}}(1 - x_{\rm c}^2)^{1/2}. \tag{2·6}$$

The GL cross section [41)] $\hat{\sigma}(Q)$ (defined as the area of such a region in the source plane that a source is lensed with certain properties Q if it resides within the region) is generally written as the integral in the y-plane:

$$\hat{\sigma}(Q) = 2\pi\eta_*^2 \int_0^\infty S(y, Q)\, y\, dy\,. \tag{2·7}$$

For example, if Q is "formation of triple images", then $S(y, Q) = \Theta(y_{\rm r} - y)$ and $\hat{\sigma} = \pi(\eta_* y_{\rm r})^2$; if Q is "image separation is larger than Δx_*" *and* "magnification is larger than μ_*" *and* "brightness ratio is smaller than r_*", then

$$\hat{\sigma}(\Delta x_*, \mu_*, r_*) = \eta_*^2\, \Theta(2x_{\rm t} - \Delta x_*)\sigma(\mu_*, r_*)\,, \tag{2·8}$$

where

$$\sigma(\mu_*, r_*) := 2\pi \int_0^{y_{\rm r}} dy\, y\, \Theta\left(\mu(y) - \mu_*\right)\, \Theta\left(r_* - r(y)\right)\,. \tag{2·9}$$

2.2. *Distance formula*

The angular diameter distances $(D_{\rm OL}, D_{\rm OS}, D_{\rm LS})$ are given by the solutions of the Dyer-Roeder equation [45),46),47)]:

$$\left[\frac{d^2}{dz^2} + \frac{3 + q(z)}{1 + z}\frac{d}{dz} + \frac{3}{2}\frac{\tilde{\alpha}\Omega(z)}{(1 + z)^2}\right] D = 0\,, \tag{2·10}$$

where $q := \frac{1}{2}\Omega - \lambda$ is the deceleration parameter, and the "smoothness parameter" $\tilde{\alpha}$ $(0 < \tilde{\alpha} < 1)$ measures the degree of inhomogeneity of the universe (for derivation, see Ref. [41)]). The last term of Eq.(2·10), the Ricci focusing term, represents the matter density inside the beam of photons. Denoting $D_{\tilde{\alpha}}(z_*, z)$ as the distance from z_* to z $(> z_*)$, the initial conditions of the differential equation (2·10) are

$$D_{\tilde{\alpha}}(z_*, z_*) = 0, \quad \frac{d}{dz} D_{\tilde{\alpha}}(z_*, z)\,\Big|_{z=z_*} = \frac{1}{(1 + z_*)H(z_*)}. \tag{2·11}$$

In particular, we write $D_{\tilde{\alpha}}(z) := D_{\tilde{\alpha}}(0, z)$. The solution with $\tilde{\alpha} = 1$ is the "filled-beam distance," and gives the standard angular diameter distance in an exactly homogeneous FRW space-time [48)], while

that with $\tilde{\alpha}=0$ is the "empty-beam distance." In the derivation of Eq.(2·10), it is assumed that the focusing due to the tidal shear (Weyl focusing) is negligible. It is shown [49),50),51)] that this assumption is plausible in most astronomical situations. In appendix A, we present specific solutions of Eq.(2·10).

2.3. *GL probability formula*

The probability that a source at redshift $z_{\rm s}$ is lensed with properties Q is generally written as [41)]

$$P(Q,z_{\rm s})=\frac{1}{D_1^2(z_{\rm s})}\int_0^{z_{\rm s}}dz\,\frac{(1+z)^2}{H(z)}D_1^2(z)\int d\chi\,\hat{\sigma}(Q,\chi,z,z_{\rm s})N_\chi(\chi,z) \tag{2·12}$$

where the integral variables z and χ are, respectively, the redshift and the parameter of the lensing objects, with the latter completely characterizing their properties (χ is not necessarily a one dimensional quantity), and $N_\chi(\chi,z)d\chi$ is the "χ-function", i.e., the comoving number density of lensing objects with the parameter $\chi\sim\chi+d\chi$ at z (the reason why the filled-beam distances are used in Eq.[2·12] is discussed in §5.1).

In the above lens model (Eq.[2·1]), the lensing cross section is characterized by a single parameter v (assuming that $\xi_{\rm c}$ is empirically related to v as Eq.[2·16]). This is why VF plays a fundamental role in the calculation of GL probability. Substituting Eq.(2·8) into Eq.(2·12), the probability that a source at $z_{\rm s}$ is multiple-imaged with image separation angle larger than θ *and* total magnification larger than μ_* *and* the brightness ratio smaller than r_* is

$$P(\theta,\mu_*,r_*,z_{\rm s})=\frac{16\pi^2}{D_1^2(z_{\rm s})}\int_0^{z_{\rm s}}dz\,\frac{(1+z)^2}{H(z)}D_1^2(z)D_{\tilde{\alpha}}^2(z,z_{\rm s})\int_{v_1}^{v_2}dv\,v^4N_v(v,z)\sigma(\mu_*,r_*)\,, \tag{2·13}$$

The limits v_1 and v_2 ($>v_1$) of the v-integral are determined by Eq.(2·6) (see Eq.[B·1]). If $x_{\rm c}(v)$ does not increase with v (i.e., $\xi_{\rm c}$ increases less rapidly than $\propto v^2$), v_1 is given by the sole positive solution of Eq.(2·6) for given θ, and $v_2=\infty$ formally (Strictly speaking, setting $v_2=\infty$ is inconsistent with the isothermal lens model because the isothermal profile does not continue to infinite radii. However, one can show that a truncation of isothermal profile at the virial radius makes little difference). If $x_{\rm c}(v)$ increases with v, then v_1 and v_2 are two positive solutions of Eq.(2·6). Probability distribution of the image separation angle is

$$P_\theta(\theta,\mu_*,r_*,z_{\rm s}):=-\frac{d}{d\theta}P(\theta,\mu_*,r_*,z_{\rm s}) \tag{2·14}$$

$$=\frac{16\pi^2}{D_1^2(z_{\rm s})}\int_0^{z_{\rm s}}dz\frac{(1+z)^2}{H(z)}D_1^2(z)D_{\tilde{\alpha}}^2(z,z_{\rm s})\left[\frac{dv}{d\theta}v^4N_v(v,z)\sigma(\mu_*,r_*)\right]_{v_2}^{v_1}. \tag{2·15}$$

Assuming

$$\xi_{\rm c}=\xi_{\rm c*}v^p\,, \tag{2·16}$$

$dv/d\theta$ in Eq.(2·15) is calculated from Eq.(2·6) as

$$\frac{dv}{d\theta}=\frac{v}{\theta}\frac{1-x_{\rm c}^2(v)}{2-px_{\rm c}^2(v)}\,. \tag{2·17}$$

In §5.2, we will see that observations suggest $p\sim3$. In appendix B, we give analytic expressions for v_1 and v_2 in the cases $p=0,1,2,3$ and 4.

2.4. *Magnification bias*

Because GL causes a magnification of images and bright QSO's are easy to discover, lensed QSO's have relatively high probability of being included in a QSO sample. This selection effect (magnification bias [52)]) is computed as follow. Let $\Phi_L^{\rm Q}(L)dL$ be the luminosity function of sources,

and let $\Phi_{\rm Q}(L) := \int_L^\infty \Phi_L^{\rm Q}(L')dL'$. When one searches for lensed QSO's of the observed flux brighter than S, the GL probability increases as [53]:

$$P_\theta^{\rm B}(\theta, S, r_*, z_{\rm s}) := \frac{1}{\Phi_{\rm Q}(L)} \int_1^\infty d\mu_* P_{\theta\mu_*}(\theta, \mu_*, r_*, z_{\rm s}) \Phi_{\rm Q}(L\bar{\mu}/\mu_*)\,, \tag{2·18}$$

where $P_{\theta\mu_*} := -(d/d\mu_*)P_\theta$, $\bar{\mu} := [D_{\tilde{\alpha}}(z_{\rm s})/D_1(z_{\rm s})]^2$, and the luminosity

$$L := 4\pi(1+z_{\rm s})^4 D_1^2(z_{\rm s})(1+z_{\rm s})^{\gamma-1}\, S \tag{2·19}$$

must be calculated from S in the same way as in the determination of $\Phi_L^{\rm Q}(L)$. The last factor $(1+z)^{\gamma-1}$ is the K-correction [54], which assumes that the energy spectrum of QSO's is of the form $E \propto \nu^{-\gamma}$. We put the factor $\bar{\mu}$ in Eq.(2·18) because the "unlensed" sources are also magnified (if $\tilde{\alpha} < 1$) by that factor on average from the flux conservation [55]. Substituting Eq.(2·15) into Eq.(2·18), the biased probability $P_\theta^{\rm B}$ is expressed as Eq.(2·15) with $\sigma(\mu_*, r_*)$ replaced by (cf. Eq.[2·9]):

$$\sigma_{\rm B}(S, r_*) := \frac{2\pi}{\Phi_{\rm Q}(L)} \int_0^{y_{\rm r}} dy\, y\, \Theta\left(r_* - r(y)\right)\, \Phi_{\rm Q}\left(\frac{\bar{\mu}L}{\mu(y)}\right)\,. \tag{2·20}$$

Similarly, for a QSO of observed flux S, the GL probability is given by Eq.(2·15) with $\sigma(\mu_*, r_*)$ replaced by*)

$$\sigma_S^{\rm B}(S, r_*) := \frac{2\pi}{\Phi_L^{\rm Q}(L)} \int_0^{y_{\rm r}} dy\, y\, \Theta\left(r_* - r(y)\right)\, \Phi_L^{\rm Q}\left(\frac{\bar{\mu}L}{\mu(y)}\right) \frac{\bar{\mu}}{\mu(y)} \tag{2·21}$$

The observed QSO luminosity function is fitted by the two power-law model [56]

$$\Phi_L^{\rm Q}(L)dL = \phi_*[(L/L_*)^\alpha + (L/L_*)^\beta]^{-1}(dL/L_*) \tag{2·22}$$

with the luminosity evolution

$$L_*(z_{\rm s}) = L_0^*(1+z_{\rm s})^{k_{\rm L}}\,, \tag{2·23}$$

where $\alpha = 3.79$, $\beta = 1.44$, $\phi_* = 6.4\times10^{-6}h^3{\rm Mpc}^{-3}$, $k_{\rm L} = 3.15$, and the absolute B-band magnitude corresponding to L_0^* is $M_0^* = -20.91 + 5\log h$. These values are obtained from $z_{\rm s} < 2.2$ QSO sample, assuming $(\Omega_0, \lambda_0) = (1, 0)$ and $\gamma = 0.5$ in Eq.(2·19) (but the values of α and β do not depend on the assumed cosmological models). Following Ref. [57], we assume that Eq.(2·23) is valid up to $z_{\rm s} = 3$ and that, for $z_{\rm s} > 3$, $L_*(z_{\rm s}) = L_0^* 4^{k_{\rm L}}\, 3.2^{(z_{\rm s}-3)/(\alpha-\beta)}$ and $\phi_*(z_{\rm s}) = \phi_0^*\, 3.2^{-(z_{\rm s}-3)(\alpha-1)/(\alpha-\beta)}$ with the same values of the parameters. The behavior of this luminosity function at $z_{\rm s} > 3$ is such that the bright end keeps constant while the faint end slides down by a factor of 3.2 in every unit redshift. We also assume that the QSO sample in Boyle et al. [56] itself does not suffer from the magnification bias, and neglect the possible magnification due to microlensing by stars in the lensing galaxies [58].

§3. Velocity function

3.1. *Schechter VF: observational viewpoint*

Standard calculation of GL probability in most of the previous work uses VF from the observed galaxy luminosity function of Schechter form at $z = 0$:

$$N_L^{\rm Sch}(L)dL = \phi_*(L/L_*)^{-\alpha} e^{-L/L_*} dL/L_*\,. \tag{3·1}$$

*) we use $(y_{\rm r} - y)^{(3-\beta)/2}$ as an integral variable in Eqs.(2·21) and (2·20) in order to eliminate the divergence of the integrand on the radial caustics $y = y_{\rm r}$

Autofib survey [59] concludes that $\alpha = 1.09$, $\phi_* = 0.026h^3\mathrm{Mpc}^{-3}$ and the absolute magnitude corresponding to L_* is $M_* = -19.20+5\log h$ in B-band. Combining with the Tully-Fisher or Faber-Jackson relation $L/L_* = (v/v_*)^\gamma$, Eq.(3·1) yields

$$N_v^{\mathrm{Sch}}(v,0)dv = \sum_{i=\mathrm{E,S0,S}} \phi_{*i}\gamma_i \left(\frac{v}{v_{*i}}\right)^{-\gamma_i(\alpha-1)} \exp\left[-\left(\frac{v}{v_{*i}}\right)^{\gamma_i}\right]\frac{dv}{v} \tag{3·2}$$

(hereafter SchVF). Therein constant comoving number density of lensing objects, i.e., $N_v(v,z) = N_v(v,0)$, is often assumed. Using the B-band Tully–Fisher and Faber–Jackson relations in Ref. [29], one finds $(\gamma, v_*) = (2.9, 126\,\mathrm{km\,s^{-1}})$ for S galaxies, and $(\gamma, v_*) = (3.3, 175\,\mathrm{km\,s^{-1}})$ for E and S0 galaxies at the above value of L_*. The morphological composition is $\phi_{*\mathrm{E}} + \phi_{*\mathrm{S0}} = 0.44\phi_*$ and $\phi_{*\mathrm{S}} = 0.56\phi_*$ [60]. We adopt the above values.

Several problems in applying SchVF to GL statistics include: (1) SchVF counts only luminous objects though they are not the only lenses: invisible dark haloes might as well be responsible for GL. (2) It is possible that the assumption of no evolution makes the SchVF strongly affected by the local and recent property of the universe around us. In fact, Autofib survey [59] found that the luminosity function steepens with redshift up to $z = 0.75$ at the faint end. Some authors [35), 61), 62), 63)] consider specific evolution models, but their conclusions does not seem decisive in that the models include some arbitrary free parameters. [Inclusion of dark objects (1) and the evolution effect (2) into GL statistics would, in principle, lead to tighter limits on Λ.] (3) The Tully-Fisher and Faber-Jackson relations may not be universal in particular at high z. (4) SchVF has an uncertainty in the velocity dispersion of early-type galaxies by a factor 1.5 [64], which changes the GL probability by $(1.5)^2$. [See Ref. [8] for a detailed study against these arguments.] (5) Clusters of galaxies, which are not counted in SchVF, can also contribute to strong lensing of QSO's [65), 66)]. Because of these uncertainties, we would like to introduce another approach below to the computation of VF.

3.2. *Press-Schechter VF: theoretical viewpoint*

Narayan & White [27] and Kochanek [28] applied the PS mass function (see, e.g., Ref. [67] for introduction) to compute VF:

$$N_M^{\mathrm{PS}}(M,z)dM = \sqrt{\frac{2}{\pi}}\frac{\bar\rho_0}{M}\frac{\delta_{\mathrm{c0}}(z)}{\sigma(R)}\left|\frac{d\ln\sigma}{d\ln M}\right|\exp\left[-\frac{\delta_{\mathrm{c0}}^2(z)}{2\sigma^2(R)}\right]\frac{dM}{M}\,, \tag{3·3}$$

where

$$\sigma(R) = \frac{1}{2\pi^2}\int_0^\infty dk\, k^2 P(k) W^2(kR) \tag{3·4}$$

is the rms of linear density fluctuation today on the comoving scale $R = [2M/(\Omega_0 H_0^2)]^{1/3}$ [$P(k)$ and $W(kR)$ are the power spectrum at $z = 0$ and the k-space window function] and $\delta_{\mathrm{c0}}(z)$ is the critical density contrast extrapolated linearly to today in order to virialize by z (Eq.[C·30]). Assuming the isothermality of the lensing objects again, the one-dimensional velocity dispersion is related to the mass through

$$v = \left[\frac{M}{2r_{\mathrm{v}}}\right]^{1/2} = \frac{1}{2}[\Omega_0\vartheta_{\mathrm{v0}}^{1/3}(z)]^{1/2}H_0 R \tag{3·5}$$

where r_{v} is the virial radius of the object and $\vartheta_{\mathrm{v0}}(z) := (R/r_{\mathrm{v}})^3$ is the overdensity of an object at $z = 0$ which virialized at z (Eq.[C·29]). Calculation of δ_{c0} and ϑ_{v0} in $\lambda = 0$ universe is found in Ref. [26]. We give analytic formulae for them in $\Omega + \lambda = 1$ universe in appendix C, using the spherical collapse model. We normalize $\sigma(R)$ so that $\sigma(8h^{-1}\mathrm{Mpc}) = b^{-1}$ (b is the bias parameter) and use the top-hat window function $W(x) = 3(\sin x - x\cos x)/x^3$. From Eqs.(3·3) and (3·5), VF is constructed

theoretically as [68),69)] (hereafter PSVF):

$$N_v^{\rm PS}(v,z)dv = \frac{3}{(2\pi)^{3/2}}\frac{1}{R^3}\frac{\delta_{\rm c0}(z)}{\sigma(R)}\left|\frac{d\ln\sigma}{d\ln R}\right|\exp\left[-\frac{\delta_{\rm c0}^2(z)}{2\sigma^2(R)}\right]\frac{dv}{v} \tag{3·6}$$

with the v-R relation in Eq.(3·5). PSVF, by its construction, properly counts all gravitationally bound objects (including the clusters of galaxies) as well as luminous objects, and automatically takes account of the hierarchical evolution of objects in the universe for various cosmological parameters [26)]. The theoretical foundation of the PS mass function is now more secure [70)] and it is also supported by cosmological N-body simulations [71),72)].

PSVF strongly increases with Ω_0 and weakly dependent on λ_0. The former is because the comoving scale R is smaller for larger Ω_0 for fixed v (Eq.[3·5]): since the density fluctuation is large on small scales [$\sigma(R)$ is large], larger Ω_0 universes have more objects at fixed v. The latter is because $\delta_{\rm c0}$ and $\vartheta_{\rm v0}$ do not so much depend on λ_0 at low redshifts. At higher redshifts, however, $\delta_{\rm c0}$ and $\vartheta_{\rm v0}$ are more dependent on λ_0 and so is PSVF. The bias parameter b affects PSVF most strongly: since $\sigma(R)\propto b^{-1}$, PSVF behaves like $\propto b\exp(-b^2)$. The dependence on h and $\Omega_{\rm B}$ is very weak because they enter only through Γ (see Eq.[4·1])

3.3. *Formation rate in theoretical VF*

PSVF is derived on the assumption that all objects have just virialized at the moment when one evaluates VF [73),74)] (see the definition of $\vartheta_{\rm v0}$). In the application to GL statistics here, this means that the deflection of light and the formation (virialization) of the deflector occurs simultaneously. In reality, however, a virialized object survives for some time until it is merged into more massive objects [26),75)], and hence there must be an accumulation of objects in a specific velocity range which formed at some earlier epochs. Therefore, we must take account of the formation epoch distribution of objects in the universe to avoid the above assumption.

Kitayama & Suto [75)] proposed a practical prescription in obtaining the formation epoch distribution from the random-walk method [70)], and calculated theoretically the comoving number density $F(M,z_{\rm f},z)dMdz_{\rm f}$ of those objects which formed at $z_{\rm f}\sim z_{\rm f}+dz_{\rm f}$ with mass $M\sim M+dM$ *and* survive without destructed (absorbed into larger hierarchies) until z. Integrating over $z_{\rm f}$, more realistic VF may be written as (hereafter KSVF):

$$N_v^{\rm KS}(v,z)dv = dv\int_z^\infty dz_{\rm f}F(M,z_{\rm f},z)\frac{dM}{dv}\,. \tag{3·7}$$

The explicit form of F is found in their Eq.(23). Compared with PSVF, KSVF is shifted to the direction of larger velocity relative to PSVF, especially on small scales (see Figs.1 and 2). This is due to the accumulation of objects, as mentioned above: because smaller objects (at $z=0$) are likely to have formed earlier in the bottom up scenario, and because older objects have higher velocities (see Eq.[3·5]), the velocity of small objects becomes larger when we take the formation history into account. Eq.(3·7) refines the original PSVF in the sense that the formation epoch is taken into account, though not fully satisfactorily [75)].

§4. Comparison with observation

4.1. *Comparison with observed VF*

In this section, we compare theoretical VF in §3 with the observed one at $z=0$ [29)]. We consider four specific cosmological models listed in Table I. The first three models (SC, OC and LC) use the scale invariant ($n=1$) power spectrum of the cold dark matter (CDM) model in Ref. [76)], and the last model (LP) uses that of the primeval isocurvature baryon [25)] (PIB) model in Ref. [77)] with the slope

Table I. Model parameters

Model	$P(k)$	Ω_0	λ_0	h	b^{-1}	$\Omega_{\rm B}h^2$
SC	CDM	1	0	0.5	1.3	0.016
OC	CDM	0.3	0	0.7	0.52	0.016
LC	CDM	0.2	0.8	0.8	1.0	0.016
LP	PIB	0.2	0.8	0.8	1.0	0.128

$n = -1.15$ at the large wavenumber. The Hubble constant h in each model is chosen so that the age of the universe be longer than 13 Gyr [21] for given (Ω_0, λ_0). The bias parameters b adopts the COBE DMR 2yr data normalization [78], and the baryon density parameter $\Omega_{\rm B}$ in the CDM models is from the big-bang nucleosynthesis constraint [79]. The Γ parameter in the CDM model is empirically fitted as [78]:

$$\Gamma = \Omega_0 h (T_0/2.7{\rm K})^{-2} \exp[-\Omega_{\rm B}(1+\sqrt{2h}/\Omega_0)] \qquad (4\cdot1)$$

where $T_0 \simeq 2.726$K is the temperature of the cosmic microwave background.

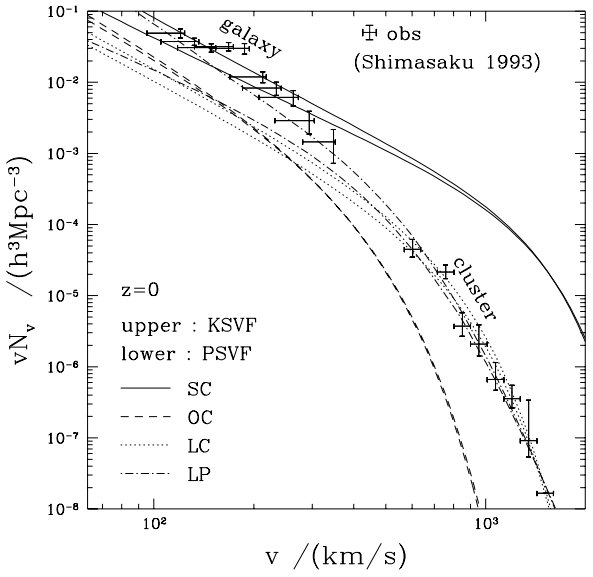

Fig. 1. PSVF (Eq.[3·6]) and KSVF (Eq.[3·7]) in the cosmological models listed in Table I. Crosses show the observed VF in Ref. [29].

In Fig.1, we plot the theoretical VF's (PSVF and KSVF) for these models at $z = 0$. In $\Omega + \lambda = 1$ case, we used the fitting formulae for $\delta_{\rm c0}$ and $\vartheta_{\rm v0}$ in Eqs.(C·19) and (C·33). Plotted in crosses are the observed VF compiled by Shimasaku [29]. He multiplied the observed central velocity dispersion of stars in E and S0 galaxies by a $1.5^{1/2}$ factor to take account of the difference between the distributions of luminous matter and isothermal dark halos. Since the error bars in the raw data represent the statistical ones only, we lengthened the error bars of galaxy VF by the $1.5^{1/2}$ factor into the smaller velocity direction. However, it should be cautioned that this is an over-modification, especially at the low velocity end, because S galaxies do not have the factor. The cluster VF is translated from the observed temperature function of Ref. [80] through the isothermal β-model assuming $\beta = 1$.

At least the VF observation should give a lower bound of the theoretical VF because the observed VF counts only luminous objects. In Fig.1, model SC fits the galaxy VF fairly well, but predicts too many large scale objects. Model OC fails on all scales due to the small value of the normalization b^{-1} from the COBE data. Models LP and LC are very good on cluster scale but significantly underpredict

galactic size objects, except for the KSVF in model LP. Shimasaku [29] also compared PSVF with the observation, and concluded that no COBE normalized models are consistent with VF observation within PSVF. However, as noted in §3.3, PSVF has a flaw: PSVF neglects the accumulation of objects which formed earlier. Although KSVF and PSVF are not so different within the CDM models, they differ significantly in model LP. This originates from the fact that the PIB models have more powers on small scales than CDM models have: since smaller objects survive longer, the accumulation in PIB models is more remarkable than that in CDM models, especially on small scales.

Nearly on all scales, KSVF in model LP seems consistent with observation if we allow the error bars to exclude the $1.5^{1/2}$ factor. However, it should be borne in mind that there underlies a lot of uncertainties both in theory and observation of VF. On the observational side: (1) The $1.5^{1/2}$ factor is quite generous and may represent the error considerably larger than the actual one. (2) Although the galaxies in the Virgo cluster is excluded in the Shimasaku [29] data, it is possible that the galaxies in small groups are counted as individual objects in that data. From the construction of theoretical VF's, a group of galaxies should be counted as one object and the galaxies inside should be neglected. (3) The assumption of $\beta = 1$ for cluster VF may not be justified because of the β-discrepancy problem [81]. (4) The observed VF may not represent the cosmic mean. On the theoretical side: (5) KSVF has some problems in counting argument [75]. (6) We have not taken any dissipative processes into account in the dynamics of virialization, both in PSVF and KSVF. That is, we have related mass with velocity (Eq.[3·5]) only from a virial analysis and neglected a possible dissipation of energy from the collapsing object.

Here let us discuss the last point (6) at some length. If one takes these dissipative processes into account, the velocity may increase because of the contraction to smaller radii. Based on the arguments of cooling and dynamical time scales [82), 83)], these effects are expected to be unimportant on cluster scales. On galactic scales where the cooling is likely to be effective, theoretical VF will shift to the right and should become steeper as compared with the dissipationless case. This line of arguments might make the model LC consistent with the observed VF. We do not estimate here quantitatively to what extent the dissipation modifies the theoretical VF, but only note that the degree of dissipative effects in the galaxy formation can be measured by comparing the observed VF with the theoretically best VF without dissipation.

In considering GL statistics, it is desirable to use VF's which are theoretically well-motivated and consistent with the observed VF. In particular, the evolution of the VF's is important in the calculation below. If one adopts the observed VF, however, one has to assume an ad-hoc number evolution. Given those uncertainties and problems, we have decided to apply theoretical and observed VF's in computing the GL probabilities on an equal basis. Further comparison between the theory and observation of VF should wait for future VF observation at higher redshifts.

In Fig.2 we plot the number evolution of PSVF and KSVF for the cosmological models in Table I. The decrease of small scale objects is slower in KSVF than that in PSVF, especially in models LC and LP. This is because the accumulation of small objects becomes less significant for higher redshifts in KSVF. The two VF's become almost identical at the redshift of ~ 4. Recently, Mo & Fukugita [84] compared PSVF with the abundance of giant galaxies at $z = 3$, and conclude that the spatially flat CDM models with $\lambda_0 \sim 0.7$ are favorable. However, their conclusion seems premature in that the model is already inconsistent with observation at $z = 0$ (Fig.1).

4.2. *Comparison with the HST snapshot survey*

Let us now calculate the GL probability in the $\xi_c = 0$ (SIS lens model) case, and compare the result with the observed GL frequency in the *HST snapshot survey* [85), 86), 87), 30)]. Various uncertainties including the non-zero core radius are examined in the next section. Although there exist different surveys in optical band [88), 89), 90)], we do not mix these data to obtain the larger number of samples [8)] because we are mainly concerned with how the results are affected by various uncertainties described

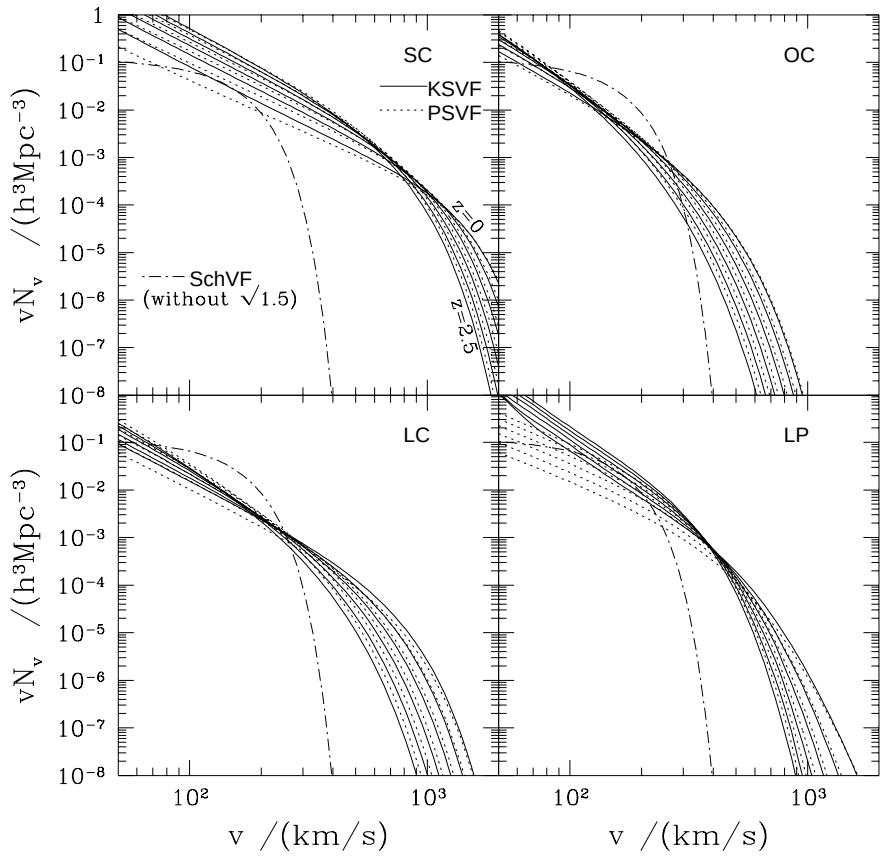

Fig. 2. Evolution of KSVF (solid) and PSVF (dotted) for the cosmological models listed in Table I. SchVF without $1.5^{1/2}$ is also shown in dot-dashed curve for reference. From upper to lower curves in high velocity end, $z = 0$, 0.5, 1, 1.5, 2, 2.5.

in §4.1 and §5.

Using the redshifts and V-band magnitudes of all the 502 QSO's in the HST survey, we calculate the expected number of lensed QSO's in the survey for various cosmological parameters as

$$n_\theta^{\rm exp}(\theta) := \sum_{i=1}^{502} P_\theta^{\rm B}(\theta, S_i, r_{*i}, z_i) \tag{4·2}$$

with Eqs.(2·18) and (2·21), where S_i and z_i are the observed V-band flux and redshift of the i-th QSO in the survey. The HST survey can detect multiple images if $\theta > 0.1''$ and if the brightness ratio is smaller than [7)]

$$r_{*i} = \min[19(\theta/{\rm arcsec})^{0.85}, S_i/S_{\rm lim}, 40]\,, \tag{4·3}$$

where $S_{\rm lim}$ is the faintest flux that the HST can detect (the corresponding apparent magnitude is $m_{\rm lim} = 22$ in V-band). We assume $B - V = 0.2$ [85)] when the V-band magnitudes are inserted into the B-band QSO luminosity function Eq.(2·22). The luminosities L_i of QSO's are calculated from S_i by Eq.(2·19) with $(\Omega_0, \lambda_0) = (1, 0)$ and $\gamma = 0.5$ [56), 91)]. We use the standard angular diameter distance ($\tilde{\alpha} = 1$; filled beam) for $D_{\tilde{\alpha}}(z, z_{\rm s})$ in Eq.(2·15).

Fig.3a shows the prediction based on SchVF, while in Fig.3b we plot the PSVF and KSVF predictions for the model parameters listed in TableI. In models OC and LC, the KSVF and PSVF predictions are almost indistinguishable (see Fig.1). Shown in the histogram is the distribution of the

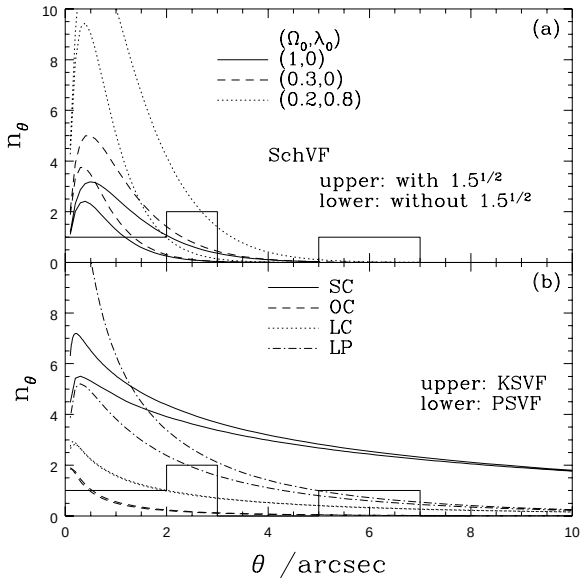

Fig. 3. Image separation distribution of the expected number of lensed QSO's in the HST survey. (a): predictions from SchVF. (b): predictions from PSVF and KSVF. Model parameters in (b) are listed in Table I. Histogram shows the observed distribution. SIS lens model ($\xi_c = 0$) and the filled-beam distance ($\tilde{\alpha} = 1$) are used.

observed 6 GL candidates in the HST survey. These are 1208+1011, 1413+117, 1115+080, 0142−100, 0957+561, 1120+0154, and the image separation angles are 0.47″, 1.22″, 2.0″, 2.2″, 5.7″ and 6.6″, respectively. Despite the high resolution imaging of the HST Planetary Camera, 1208+1011 is the only sub-arcsecond GL candidate found by the survey [92), 93)].

Note that the SchVF can never predict the large separation lensing events such as 0957+561 and 1120+0154, even if the $1.5^{1/2}$ factor is included. Usually these large separation events are neglected as statistical flukes in the literatures of GL statistics based on SchVF. Maoz & Rix [7)], for example, neglects 0957+561 because it is not the lensing by a single galaxy but the lensing galaxy may be embedded in a cluster [94)]. They also neglect 1120+0154 because the images might be a physical pair (however, see Refs. [95), 96)]). However, we believe that it is important to consider these large separation lensing events when the PSVF or KSVF predictions are compared with observation, because the theoretical VF's in principle count all the gravitationally bound dark objects as well as luminous objects. The apparent absence of any obvious lensing object in 1120+0154 may be due to such non-luminous massive objects.

It is also interesting to note that the predictions from observed VF and theoretical VF have opposite dependence on Ω_0. This is because theoretical VF naturally decreases with Ω_0 (low density universe has fewer lenses). On the contrary, since SchVF does not at all depend on the cosmological parameters but is fixed by observation, the Ω_0 and λ_0 dependence of SchVF prediction enters only through the cosmological geometry (distance formulae and the Hubble constant). In the case of PSVF and KSVF predictions, the λ_0 dependence comes mainly from the COBE normalized bias parameter b.

Fig.3a shows that the SchVF prediction apparently prefers $\Lambda = 0$ models to highly Λ-dominated models [5), 6), 7), 8)]. In Fig.3b, model SC predicts too many lensing events in all separation range [28)]. Again model OC is not viable: the COBE normalized density fluctuation amplitude b^{-1} in this model is too small to accommodate sufficient lensing objects. The most likely values of Ω_0 in open universes should lie between 0.3 and 1. Model LC seems relatively good, while model LP is good at large separations but too much overpredicts the small separation events. We tabulate in Table II the expected number $n_{\rm exp} := \int n_\theta^{\rm exp}(\theta) d\theta$ of lensed sources for these models, and their χ^2 significance

level [97]

$$Q := \frac{\Gamma(n_{\rm bin}/2, \chi^2/2)}{\Gamma(n_{\rm bin}/2)}, \quad \chi^2 := \sum_{i=1}^{n_{\rm bin}} \frac{(n_i^{\rm obs} - n_i^{\rm exp})^2}{n_i^{\rm exp}}, \tag{4·4}$$

where $n_i^{\rm obs}$ and $n_i^{\rm exp}$ are the observed and expected number of lensed sources in the i-th bin. We set the bin width to be $\Delta\theta_{\rm bin} = 1''$ as shown in Fig.3, and calculate $n_{\rm exp}$ and Q within the separation range $0'' < \theta < 4''$ for SchVF predictions, and within $0'' < \theta < 10''$ for PSVF and KSVF predictions (see the first row of the table denoted as "standard").

We note that, if the $1.5^{1/2}$ factor is excluded, the $\Lambda = 0$ models in the SchVF prediction have very low significance level, because these models do not predict sufficient number of lensed QSO's around $\theta \sim 2''$ (1115+080 and 0142−100). If the $1.5^{1/2}$ factor is included, the values of Q in $\Lambda = 0$ models are larger than those in $\Lambda \neq 0$ models *only relatively*: no models in the SchVF prediction can fit the observed distribution satisfactorily. The maximum likelihood analysis [98] is unable to show this fact, where only the relative values of the likelihood among the models are calculated. This is why we do not use the likelihood analysis for the cosmological parameters.*) We caution, however, that the probabilities in the table are not statistically so meaningful because of the small number of lensed candidates. More reliable tests will be possible after the next-generation GL samples become available (see §6).

As seen from Fig.3 and Table II, GL statistics based on theoretical VF's prefers spatially flat low density models with the non-vanishing cosmological constant (if COBE normalized), as opposed to the SchVF prediction (this is consistent with the results in Ref. [66] which focused on the large separation lensing statistics using the observed cluster mass function in Ref. [12]). In particular, the model LC matches the observation fairly well. However, this is originated from the fact that the VF itself in the model LC underpredict the number of galaxy scale lenses today (Fig.1). Although the KSVF in model LP is the only theoretical VF (among the four models) consistent with the VF observation in Fig.1, Fig.3b shows that the KSVF prediction of the model LP is unfavorably larger than the observed events at small separations.

As discussed in §4.1 the observed VF on galaxy scales may be affected by dissipative effects. However, it is not clear which the observed VF or the theoretical VF without dissipation is relevant for GL statistics: if the lensing objects cannot be modeled as isothermal, then it might well be that the observed velocity dispersion in their central parts is larger than the effective value of v inside the Einstein radius of the isothermal model. If this is the case, the observed VF will overestimate the deflection angle and so the GL cross section. In passing we note that, if the observed VF is affected by dissipative effects, and if theoretical VF's without dissipation is relevant for GL statistics, then the model LC may become consistent with both of the VF and GL observations.

§5. Various uncertainties in GL statistics

Within the SIS lens model and the standard distance formula ($\tilde{\alpha} = 1$), we could not find a cosmological model which satisfies both GL and VF observations. In this section we consider various uncertainties (free parameters) in the predictions of GL statistics. The results are summarized in Table II

5.1. *Distance formula*

We have no knowledge at present as to what value of the smoothness parameter $\tilde{\alpha}$ in the distance formula (Eq.[2·10]) describes our universe best. First of all, it is important to realize that the distances appearing in the lens equation (Eq.[2·2]) and the GL probability formula (Eq.[2·12]) has slightly

*) We do use the Kolmogorov–Smirnov test here because we want to compare the amplitude of the observed event rate with that of the theoretical predictions. This is also why we use the χ^2 test although the binning is very crude.

Table II. The expected number $n_{\rm exp}$ of lensed QSO's in the HST snapshot survey and the χ^2 significance level Q (Eq.[4·4]) of the models (see Table I). (a,b): SchVF predictions within the separation range $0'' < \theta < 4''$; (c): PSVF predictions within $0'' < \theta < 10''$; (d): KSVF predictions within $0'' < \theta < 10''$; are compared with the observation.

(a) VF	SchVF without $1.5^{1/2}$					
(Ω_0, λ_0)	(1,0)		(0.3,0)		(0.2,0.8)	
$0'' < \theta < 4''$ ($n_{\rm obs} = 4$)	$n_{\rm exp}$	Q	$n_{\rm exp}$	Q	$n_{\rm exp}$	Q
Standard (§4.2)	2.5	$< 0.1\%$	3.7	$< 0.1\%$	10	2.1%
Distance formula[a] (§5.1)	1.4	$< 0.1\%$	2.9	$< 0.1\%$	7.2	0.5%
Core radius[b] (§5.2)	2.3	$< 0.1\%$	3.4	$< 0.1\%$	9.4	1.2%
Magnification bias[c] (§5.3)	1.7	$< 0.1\%$	1.9	$< 0.1\%$	5.3	0.5%
Dust obscuration[d] (§5.4)	1.8	$< 0.1\%$	2.7	$< 0.1\%$	7.8	4.2%

(b) VF	SchVF with $1.5^{1/2}$					
(Ω_0, λ_0)	(1,0)		(0.3,0)		(0.2,0.8)	
$0'' < \theta < 4''$ ($n_{\rm obs} = 4$)	$n_{\rm exp}$	Q	$n_{\rm exp}$	Q	$n_{\rm exp}$	Q
Standard (§4.2)	5.1	38%	7.5	30%	20	0.7%
Distance formula[a] (§5.1)	2.8	3.7%	5.9	25%	15	5.2%
Core radius[b] (§5.2)	4.4	26%	6.5	26%	18	1.5%
Magnification bias[c] (§5.3)	2.6	9.1%	3.8	19%	11	19%
Dust obscuration[d] (§5.4)	4.1	45%	6.0	43%	17	2.7%

(c) VF	PSVF							
Model	SC		OC		LC		LP	
$0'' < \theta < 10''$ ($n_{\rm obs} = 6$)	$n_{\rm exp}$	Q	$n_{\rm exp}$	Q	$n_{\rm exp}$	Q	$n_{\rm exp}$	Q
Standard (§4.2)	29	3.2%	1.7	$< 0.1\%$	6.1	79%	16	45%
Distance formula[a] (§5.1)	17	55%	1.3	$< 0.1\%$	4.6	48%	9.3	81%
Core radius[b] (§5.2)	18	44%	1.6	$< 0.1\%$	5.4	55%	11	73%
Magnification bias[c] (§5.3)	23	17%	1.4	$< 0.1\%$	5.1	60%	11	79%
Dust obscuration[d] (§5.4)	27	6.5%	1.3	$< 0.1\%$	5.7	79%	12	79%

(d) VF	KSVF							
Model	SC		OC		LC		LP	
$0'' < \theta < 10''$ ($n_{\rm obs} = 6$)	$n_{\rm exp}$	Q	$n_{\rm exp}$	Q	$n_{\rm exp}$	Q	$n_{\rm exp}$	Q
Standard (§4.2)	32	1.3%	1.6	$< 0.1\%$	6.0	77%	21	18%
Distance formula[a] (§5.1)	18	43%	1.2	$< 0.1\%$	4.5	47%	14	58%
Core radius[b] (§5.2)	21	27%	0.7	$< 0.1\%$	5.4	53%	19	20%
Magnification bias[c] (§5.3)	22	23%	1.0	$< 0.1\%$	4.2	40%	13	62%
Dust obscuration[d] (§5.4)	29	3.4%	1.2	$< 0.1\%$	5.6	77%	19	33%

[a] Self-consistent formula with $\tilde{\alpha} = 0$ is used.

[b] $\xi_{\rm c} = 0.2(v/200\,{\rm km\,s^{-1}})^3 h^{-1}{\rm kpc}$.

[c] Magnification of only the brighter image is used.

[d] $\tau_{\rm cV} = 1$, $\xi_{\rm d} = 0.3h^{-1}{\rm kpc}$.

different meanings. First let us discuss why the filled beam ($\tilde{\alpha} = 1$) distances are used in Eq.(2·12).

Actually Eq.(2·12) has two different derivations. One is the "self-consistent" formula[31] which uses $\tilde{\alpha} = 1$ in the GL probability formula (as in Eq.[2·12]), and the other is the "optical-depth" formula[99),53] which do not distinguish the distances in Eqs.(2·2) and (2·12), and use the same value of $\tilde{\alpha}$ in both the equations. In the self-consistent formula, the lensing cross section is defined in the source plane (as in Eq.[2·7]) and the GL probability is defined by the ratio of the total lensing cross section to the whole area of survey regions in the source plane. In this case, the distances in Eq.(2·12)

measure the proper area in the lens and source planes subtended by the solid angle of the regions. Thus, if one observes GL frequency in the whole 4π steradians in the sky, the filled beam distances should be used in Eq.(2·12) because (we assume) the universe is on average homogeneous. On the other hand, in the optical-depth formula, the lensing cross section is defined in the lens plane and the GL probability is defined by the mean number of deflections along line-of-sight. Since $D_1(z_{\rm s})/D_{\tilde{\alpha}}(z_{\rm s}) \leq 1$, the optical depth formula is always smaller than the self-consistent formula [31),6)] and the difference becomes larger for smaller $\tilde{\alpha}$, larger $z_{\rm s}$, Ω_0 and λ_0. For example, when $\tilde{\alpha} = 0$, $(\Omega, \lambda) = (1, 0)$, and $z_{\rm s} = 2$, the two GL probabilities differ by a factor of 0.645. We adopt the self-consistent formula because, as pointed out in Ref. [31)], the line-of-sight cannot be treated as a random variable but the source position on the source plane can be. Although the GL observation data used in §4.2 do not cover the whole 4π steradians, the survey region is wide enough to assume the statistical homogeneity [55),100)].

On the other hand, the distances appearing in the lens equation (Eq.[2·2]) measure the proper lengths in the lens and source planes on scales of the typical image separation. It is shown (Sasaki [101)]) that the choice of $\tilde{\alpha}$ in Eq.(2·2) depends on how clumpy one imagines the universe is on that scale. So $\tilde{\alpha}$ in Eq.(2·2) is a statistical quantity and may depend on the directions in the sky. Sasaki [101)] also argues that, when one calculates the deflection angle $\hat{\alpha} = (d/d\xi)\hat{\psi}$, the density profile of lensing objects should be subtracted by $\tilde{\alpha}\bar{\rho}$ for consistency because the lens potential $\hat{\psi}$ (Eq.[2·1]) is a perturbative quantity against the homogeneous background. In the case of strong lensing, however, the subtraction of $\tilde{\alpha}\bar{\rho}$ makes little difference: if we assume that the lensing object has virialized before the light passes by it, the density of the lens is at least $\vartheta_{\rm v}$ times larger than the background when the light is deflected. Since the deflection angle is roughly proportional to the mass of the lens, and since $\vartheta_{\rm v} \geq 18\pi^2$ (Eq.[C·18]), the fractional change in the deflection angle due to $\tilde{\alpha}\bar{\rho}$ is at most a factor of 10^{-2}, which is observationally negligible.

To be pedantic, setting $\tilde{\alpha} = 1$ in Eq.(2·2) is inconsistent because the strong GL cannot occur in the $\tilde{\alpha} = 1$, exactly homogeneous universe. As $\tilde{\alpha}$ decreases from unity, the GL probability (without magnification bias) increases through the geometrical effect: because of the decreasing focusing, the proper area of the GL cross section increases. The effect of $\tilde{\alpha}$ is larger for larger Ω_0 or λ_0 universes. This is because $\tilde{\alpha}$ in the Ricci focusing term (Eq.[2·10]) is multiplied by $\Omega(z)$ and larger λ_0 makes $\Omega(z)$ approach unity faster at higher redshifts. On the contrary, if the magnification bias is taken into account, the GL probability decreases as $\tilde{\alpha}$ decreases, because of the factor $\bar{\mu} := [D_{\tilde{\alpha}}(z_{\rm s})/D_1(z_{\rm s})]^2$ in Eqs.(2·21) and (2·20). However, this decrease of GL probability with $\tilde{\alpha}$ is rather artificial: intuitively, as $\tilde{\alpha}$ decreases, the universe becomes clumpy so the number of lensing objects and the GL probability should increase. It may be that the number density of lensing objects should be multiplied by $(1 - \tilde{\alpha})$ to take this effect into account.

Fig.4 is the same as Fig.3b except that $\tilde{\alpha} = 0$ (extreme case). Fig.4a shows the PSVF and KSVF predictions from the self-consistent formula, while Fig.4b uses the optical depth formula. Because of the decrease of the magnification bias mentioned above, the GL predictions decrease as compared with Fig.3. In our opinion, previous work (e.g., Ref. [6)]) might overestimate the magnification bias because of the absence of the factor $\bar{\mu}$ in Eq.(2·21): what is essential to the magnification bias is the relative magnification $\mu(y)/\bar{\mu}$ of a lensed source to unlensed sources. The χ^2 significance levels of the models are tabulated in the second row of Table II. In extremely inhomogeneous ($\tilde{\alpha} = 0$) universes the models SC and LP are viable.

5.2. *Core radius*

It is known [32)] that a small but finite core radius can change the lensing probability by an order of magnitude: since the strength of a lens is determined by its central condensation of the surface density, the removal of the central singularity reduces the lensing cross section significantly [$\propto (1 - x_{\rm c}^{2/3})^3$; Eq.(2·8)]. However, as noted in Ref. [8)], the inclusion of core radius increases the magnification bias: the significant decrease in the GL probability with the core radius is compensated to some extent

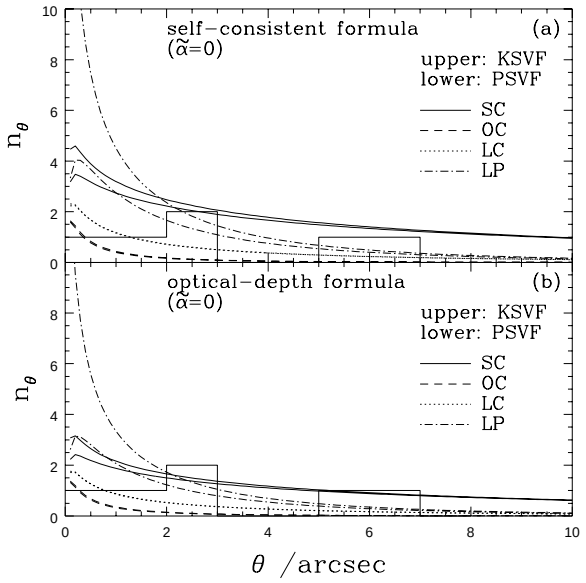

Fig. 4. Same as Fig.3b, except that the smoothness parameter (Eq.[2·10]) is $\tilde{\alpha} = 0$. (a) self-consistent formula (Eq.[2·15]) with the empty-beam distance ($\tilde{\alpha} = 0$) is used; (b): optical-depth formula with the empty-beam distance ($\tilde{\alpha} = 0$) is used in stead of Eq.(2·15).

by the increase of the magnification bias. The probability even increases with core radius when the source luminosity is greater than $\sim 20L_*$.

From Eq.(2·3), the scaled core radius $x_{\rm c}$ is written as

$$x_{\rm c} \simeq 0.72 \left[\frac{v}{100\,{\rm km\,s^{-1}}}\right]^{-2} \frac{D_{\rm OS}}{D_{\rm LS}} \left[\frac{hD_{\rm OL}}{\rm Gpc}\right]^{-1} \frac{h\xi_{\rm c}}{\rm kpc}\,. \tag{5·1}$$

On galaxy scales the core radius is rather small. Fukugita & Turner [5] estimate $\xi_{\rm c} = 324\,h^{-1}$pc at $v = 225\,{\rm km\,s^{-1}}$ from the observation of E galaxies in Ref. [102], which corresponds to $x_{\rm c} \sim 0.12$ for a lens redshift of $z \sim 0.5$. From the same data, Krauss & White [103] obtains $\xi_{\rm c} = 557\,h^{-1}$pc at $v = 306\,{\rm km\,s^{-1}}$ ($x_{\rm c} \sim 0.14$) and $\xi_{\rm c} \propto L^{0.73}$, though the scatter in the data is very large. Using the Faber-Jackson relation, one obtains $p \sim 2.9$ (see Eq.[2·16]). Wallington & Narayan [57] argues that $\xi_{\rm c}$ must be smaller than about $200\,h^{-1}$pc at $v = 225\,{\rm km\,s^{-1}}$ ($x_{\rm c} \sim 0.08$) so that the observed even number of lensed images is explained by the demagnification of the central image. On cluster scales the core radius is typically $\xi_{\rm c} \sim 20$–$30h^{-1}$kpc at $v = 1000\,{\rm km\,s^{-1}}$ which corresponds to $x_{\rm c} \sim 0.4$–0.6 [65), 66), 104)]. These data suggest that $p \sim 3$ and $\xi_{\rm c} \sim 0.2h^{-1}$kpc at $v = 200\,{\rm km\,s^{-1}}$.

Fig.5 plots the same quantities as in Fig.3b except that the finite core radius is included and only the KSVF predictions are shown. We examined $p = 1, 2$ and 3 (Eq.[2·16]), in Figs.5a, b, and c, respectively. From upper to lower of the five curves for each model, the core radius is $\xi_{\rm c} = 0, 0.1, 0.2, 0.3, 0.4h^{-1}$kpc at $v = 200\,{\rm km\,s^{-1}}$. When $p < 2$, the GL probability decreases mainly at small θ and asymptotes to the SIS ($\xi_{\rm c} = 0$) case at large θ, simply because $x_{\rm c} \propto v^{p-2}$ (Eq.[2·6]). When $p > 2$ the converse behaviour occurs, and when $p = 2$, it decreases uniformly. We note that the effect of the core radius is slightly smaller in larger λ_0 universes. This is because the scale length ξ_* (Eq.[2·3]) increases with increasing λ_0 due to the cosmological geometry: larger ξ_* means that the light traverses farther away from the lensing object, so the core radius looks effectively smaller. For the core radius of $\xi_{\rm c} = 0.2(v/200\,{\rm km\,s^{-1}})^3 h^{-1}$kpc, the χ^2 significance levels of the models are summarized in the third row of Table II.

The above estimates for the core radius of early-type galaxies are based on pre-HST data. But

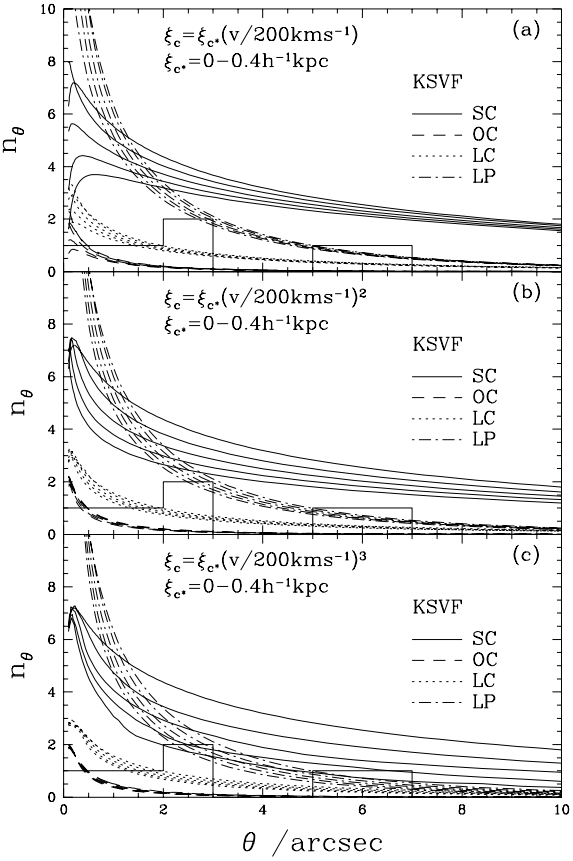

Fig. 5. Same as Fig.3b, except that the finite core radius ξ_c is included and only the KSVF predictions are shown. (a): $\xi_c = \xi_{c*}(v/200\,\mathrm{km\,s^{-1}})$; (b): $\xi_c = \xi_{c*}(v/200\,\mathrm{km\,s^{-1}})^2$; (c): $\xi_c = \xi_{c*}(v/200\,\mathrm{km\,s^{-1}})^3$; with $\xi_{c*} = 0, 0.1, 0.2, 0.3, 0.4h^{-1}$kpc from upper to lower curves.

recent observation of these galaxies by HST [105), 106)] shows that they have nearly singular cores. Moreover, Ref. [107)] argues that the inclusion of finite core radius should increase the velocity dispersion of dark matter for consistency. Based on these arguments, the effect of the core radius may be smaller than that given in Table II in practice.

5.3. *Magnification bias*

The magnification bias (Eqs.[2·21] and [2·20]) contains $\mu(y)$ which is defined in §2.1 as the total magnification of all the images. However, depending on the properties of a QSO sample or the GL configuration, $\mu(y)$ in the bias factor should be interpreted as the magnification of only the brighter image or the fainter image among the outer two images. If individual QSO's in a sample are not examined so closely whether they are lensed or not, the magnification of only the fainter image should be used [35)] because the fainter image should be bright enough to be recognized as one of the multiple images. On the contrary, if one examines the QSO's closely enough to search for the second image by a follow-up observation (as in the HST snapshot survey), the magnification of the brighter image or the total magnification should be used [108)]. Which magnification – brighter image or the total – should be used may depend on the image separation angle: if one searches for lensed sources of small separation angles, then the total magnification may be relevant, because it is likely that the brightness of a lensed source with a small separation is recognized as the total brightness of all the images.

Fig.6 shows how different choices for the magnification bias affect the GL prediction for the HST

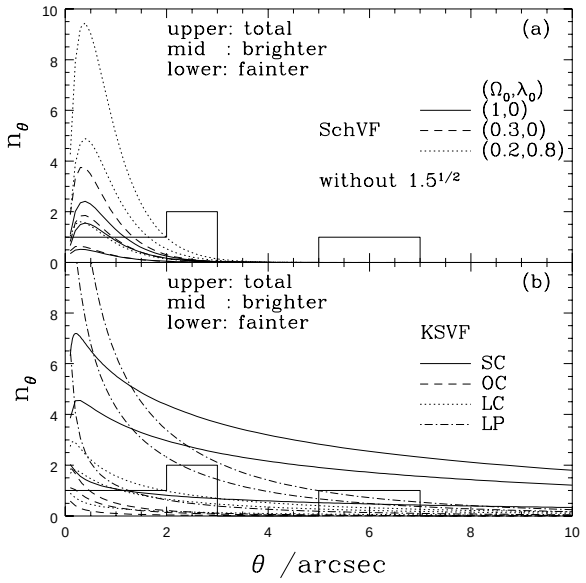

Fig. 6. Same as Fig.3, except that $\mu(y)$ in the magnification bias (2·21) is defined as the magnification of the brighter image (the middle curves) or the fainter image (lower curves) of the outer two images. The upper curves use the total magnification of all the images for $\mu(y)$ as in Fig3.

survey. The upper curves for each model use the total magnification for $\mu(y)$, while the middle and lower curves use the magnification of brighter and fainter image, respectively. Only the KSVF predictions and SchVF predictions without the $1.5^{1/2}$ factor are shown. For the middle curves, the χ^2 significance levels of the models are shown in the fourth row of Table II. Because the effect of the magnification bias is very large in the GL prediction, the different choices of the bias factor changes the result significantly.

The uncertainties in the QSO luminosity function (Eq.[2·22]), $\alpha = 3.79 \pm 0.15$, $k_{\rm L} = 3.15 \pm 0.10$ and $M_0^* = -20.91 \pm 0.25 + 5\log h$, change the GL prediction by $\sim \pm 40\%$, $\pm 40\%$ and $\pm 20\%$, respectively, while $\beta = 1.44 \pm 0.20$ does not cause significant changes because QSO's brighter than L_* are preferentially selected in the HST snapshot survey in order to achieve high efficiency of the lens detection [109].

5.4. *Dust obscuration*

When the light from a lensed source passes by the lensing galaxy, the lensed image may be obscured by the dust ingredients in the galaxy. For example, the scale length (Eq.[2·3])

$$\xi_* \simeq 1.4 h^{-1}{\rm kpc} \left[\frac{v}{100\,{\rm km\,s^{-1}}}\right]^2 \frac{D_{\rm LS}}{D_{\rm OS}} \frac{h D_{\rm OL}}{\rm Gpc} \qquad (5\cdot2)$$

is about $2h^{-1}$kpc for a lensing galaxy of $v = 200\,{\rm km\,s^{-1}}$ and $z = 0.5$, which may be well inside the baryonic parts of the galaxy. The dust obscuration reduces the GL probability in two ways: i) due to the dust demagnification, the magnification bias decreases; ii) brightness ratio of the images is amplified and so it becomes hard to detect the second image, because the fainter image, which is nearer to the lens center, is more appreciably demagnified than the brighter image.

Let us estimate this effect quantitatively by a simple model [33), 34), 8)]. Since elliptical galaxies dominate over spiral galaxies in GL statistics (§3.1), the former is considered here as lensing galaxies. Let $\tau(\xi)$ be the (2-dimensional) optical depth profile due to obscuration by dusts at the impact

parameter ξ from the center of the galaxy. We assume the following form of $\tau(\xi)$:

$$\tau(\xi) = \tau_{\rm c}/[1 + (\xi/\xi_{\rm d})^2] \tag{5·3}$$

where $\tau_{\rm c}$ is the optical depth at the center and $\xi_{\rm d}$ is the dust core radius. The light ray which passes by the lensing galaxy at ξ is demagnified by a factor $e^{-\tau(\xi)}$. Accordingly we have to redefine the total magnification $\mu(y)$ and the brightness ratio $r(y)$ in Eq.(2·21) by replacing $\mu_{\rm p}(x)$ in §2.1 with $\mu_{\rm p}(x)e^{-\tau(\xi_* x)}$, and recalculate the magnification bias. The optical depth is sensitive to the wavelength λ. Following Ref.[34], we use the fitting formula of Ref.[110]:

$$\tau_{\rm c}(\lambda) \simeq \tau_{\rm cV} X(x)/3.2\,, \tag{5·4}$$

where $x := (\lambda/\mu{\rm m})^{-1}$, $\tau_{\rm cV}$ is the optical depth in V-band ($x_{\rm V} = 1.8$), and the functional form of $X(x)$ is found in Ref.[34]. If QSO is observed in the wavelength $\lambda_{\rm obs}$ and the lensing galaxy is at redshift z, then the demagnification factor should be evaluated at the wavelength $\lambda_{\rm obs}/(1+z)$. Wise & Silva[111] obtain $\tau_{\rm cV} \sim 1$ comparing their dust model with the data of 52 elliptical galaxies. We estimate $\xi_{\rm d} \sim 0.3h^{-1}$kpc, assuming that $\xi_{\rm d}$ is 0.1 times the effective radius of the de Vaucouleurs profile[40]. To be more realistic, $\tau_{\rm cV}$ and $\xi_{\rm d}$ should be dependent on the velocity dispersion v (the sizes of galaxies) and on z (the evolution of galaxies). However, we set them constant for simplicity because we aim at examining the extent to which the dust obscuration affects the GL probability.

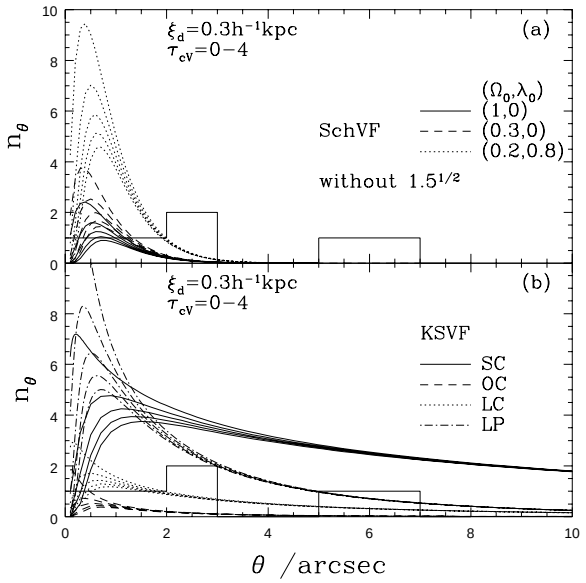

Fig. 7. Same as Fig.3, except that the dust obscuration effect by lensing galaxies is included, and only KSVF predictions and SchVF predictions without the $1.5^{1/2}$ factor are shown. From upper to lower curves, the optical depth of the dust obscuration is $\tau_{\rm cV} = 0, 1, 2, 3, 4$ (see Eq.[5·3])

Fig.7 shows the dust obscured GL predictions on the HST survey. Only KSVF predictions and SchVF predictions without the $1.5^{1/2}$ factor are shown. Among the five curves for each model, the optical depth is $\tau_{\rm cV} = 0, 1, 2, 3, 4$ from the upper to lower curves, and $\xi_{\rm d}$ is set to $0.3h^{-1}$kpc. The dust obscuration effect is considerably large at the small separation angles. We note, however, that the effect becomes small if one includes a finite core radius, because the brightness ratio becomes small. For the "realistic" value $\tau_{\rm cV} = 1$, the χ^2 significance levels of the models are presented in the fifth row of Table II.

Let us note general features of the effect of the dust obscuration. Larger λ_0 universes have smaller effect of the dust obscuration because the light rays are likely to pass by farther from the lens center,

as noted in §5.2. If $\xi_{\rm d}$ increases with v less rapidly than $\propto v^2$, the GL probability decreases mainly at small separation and asymptotes to the no-dust curve at large separation, and the converse is true if $\xi_{\rm d}$ increases more rapidly than v^2, for exactly the same reason as in Fig.5. If $\tau_{\rm cV}$ increases with z due to the star formation activities at higher redshifts [33], lensed images with small separations are more obscured than those with large separations, because the former are likely to be produced by lensing objects of high redshifts (see Eq.[2·6]). Observation [111, 112] suggest that the dusts are more diffusely distributed as $\rho_{\rm dust}(r) \propto r^{-1}$ rather than as Eq.(5·3). In this case large separation images are more obscured than in Fig.7.

§6. Predictions for future surveys

With the limited statistics of the current data, the constraints on the parameters are not yet decisive. We expect, however, that a much larger number of sources will be homogeneously sampled in one systematic lens survey in the near future. For example, the Sloan Digital Sky Survey (SDSS) plans a spectroscopic survey of 10^5 QSO's over π steradians brighter than 19 magnitude in g-band [113]. In this section, we will make predictions on future GL surveys, bearing mainly the SDSS in mind.

Let $n_\theta(\theta, S)d\theta$ be the expected number of lensed QSO's with image separation $\theta \sim \theta + d\theta$ and observed flux brighter than S, within the solid angle $\Omega_{\rm sa}$ in the sky. We assume that the survey examines all the QSO's in the sky homogeneously. Then, using the cumulative QSO luminosity function $\Phi_{\rm Q}$ in §2.4, $n_\theta(\theta, S)$ can be calculated as

$$n_\theta(\theta, S) = \Omega_{\rm sa} \int_0^{z_{\rm max}} dz \frac{dr}{dz} r^2(z) \Phi_{\rm Q}(L, z) P_\theta^{\rm B}(\theta, S, r_*, z)\,, \qquad (6\cdot1)$$

where L is related to S by Eq.(2·19), $r(z) := (1+z)D_1(z)$ is the proper motion distance from us to z, and Eqs.(2·18) and (2·20) are substituted for $P_\theta^{\rm B}$. Since we use Eq.(2·22) for $\Phi_{\rm Q}(L)$ which assumes $(\Omega, \lambda) = (1, 0)$ and $\gamma = 0.5$, these values of the parameters are also used in Eq.(2·19) and $r(z)$. We set $z_{\rm max} = 5$ [57], and use the same detection limit $r_* = 19(\theta/{\rm arcsec})^{0.85}$ as that of the HST survey.

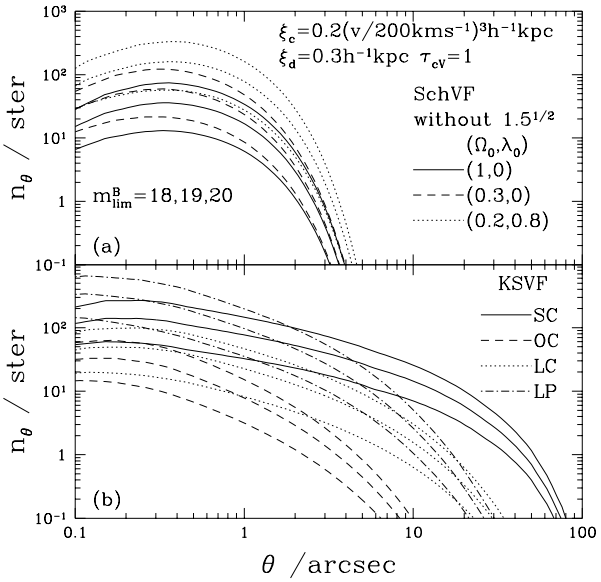

Fig. 8. Image separation θ distribution of the expected number of all the lensed QSO's per unit steradian in the sky (Eq.[6·1]). (a): predictions from SchVF. (b): predictions from KSVF. From lower to upper of the three curves for each model, the limiting magnitude is $m = 18, 19, 20$ in B-band.

Table III. The expected number of lensed QSO's per unit steradian brighter than 18, 19 and 20 B-mag. (a): SchVF predictions within the separation range $0'' < \theta < 5''$; (b): PSVF and KSVF predictions within $0'' < \theta < 5''$; (c): PSVF and KSVF predictions within $5'' < \theta < 10''$; for models in Table I. We adopt $\xi_{\rm c} = 0.2(v/200\,{\rm km\,s^{-1}})^3 h^{-1}{\rm kpc}$, $\tau_{\rm cV} = 1$ and $\xi_{\rm d} = 0.3h^{-1}{\rm kpc}$ as the models of the core radius and the dust obscuration (see §5.2 and §5.4).

$0'' < \theta < 5''$

(a)	SchVF without $1.5^{1/2}$			SchVF with $1.5^{1/2}$		
(Ω_0, λ_0)	$B < 18$	19	20	18	19	20
(1,0)	13	35	70	25	66	132
(0.3,0)	19	52	106	37	100	202
(0.2,0.8)	57	158	326	111	306	629

$0'' < \theta < 5''$

(b)	PSVF			KSVF		
Model	$B < 18$	19	20	18	19	20
SC	102	233	436	118	270	508
OC	11	27	53	10	25	48
LC	28	74	151	27	72	146
LP	65	172	348	114	305	620

$5'' < \theta < 10''$

(c)	PSVF			KSVF		
Model	$B < 18$	19	20	18	19	20
SC	43	92	165	46	97	176
OC	0.5	1.0	1.9	0.4	0.9	1.6
LC	5.6	14	28	5.4	14	27
LP	10	25	49	12	30	58

Fig.8 and Table III show the predictions on future surveys: the expected number of lensed QSO's per unit steradian ($\Omega_{\rm sa} = 1$). We adopt $\xi_{\rm c} = 0.2(v/200\,{\rm km\,s^{-1}})^3 h^{-1}{\rm kpc}$, $\tau_{\rm cV} = 1$ and $\xi_{\rm d} = 0.3h^{-1}{\rm kpc}$ as the models of the core radius and the dust obscuration, which we regard as the realistic values (see §5.2 and 5.4). The standard angular diameter distance ($\tilde{\alpha} = 1$) is used. In Fig.8, the KSVF predictions and the SchVF predictions without the $1.5^{1/2}$ factor are shown. Among the three curves for each model, the apparent limiting magnitudes corresponding to S are $m = 18, 19, 20$ in B-band from lower to upper curves. Table IIIa shows the SchVF predictions within the separation range $0'' < \theta < 5''$, while Table IIIb and IIIc show the PSVF and KSVF predictions within $0'' < \theta < 5''$ and $5'' < \theta < 10''$. The KSVF prediction is strongly dependent on Ω_0 and the bias parameter b. Therefore, we believe that Fig.8b will provide a promising test for one of these parameters if the other is given independently.

We propose that the cosmological tests should be carried out at a large separation range so that various uncertainties do not enter: the dust obscuration may be ineffective at $\theta \gtrsim 3''$ (Fig.7); theoretical VF is free from uncertainties concerning the formation rate or the dissipative processes (§4.1) at $\theta \gtrsim 7''$ (corresponding to $v \sim 500\,{\rm km\,s^{-1}}$; Eqs.[2·6] and [5·1]) which nearly discriminate the galaxy scale and cluster scale; etc. Alternatively, the lensing events with $\theta \lesssim 7''$ should provide information about VF and the dissipative effects on the dynamics of galaxy formation.

In closing we give some cautions on Fig.8. It may be that the predictions in the figure are overestimated because of the assumption that the QSO luminosity function of Boyle et al.[56] is valid up to $z = 3$. The dependences on the core radius and the dust obscuration are similar to Figs.5 and 7. The uncertainties in the values of M_0^* and k_L change the predictions by $\sim \pm 20\%$ and $\pm 10\%$. Those of α and β do not cause a significant change.

§7. Summary and conclusion

To date, it is well known that GL statistics disfavors cosmological models dominated by the positive cosmological constant Λ [5), 7), 8)], in contrast to the other cosmological tests suggesting low density universe with non-zero Λ [15), 16)]. In the light of this, we reexamined the current constraints on Λ from GL statistics, mainly paying attention to the role of VF in the calculation of GL probability.

Most previous work on GL statistics uses SchVF which counts only luminous galaxies as lensing objects. Moreover constant comoving number of lenses (no evolution) is often assumed. To take account of dark lensing objects and their number evolution, VF is constructed theoretically from the PS theory in §3 [27), 28)]. Actually the PS theory in its original form is not a perfect one in deriving VF, and we attempted in §3.3 to construct a more realistic VF (KSVF) from the hierarchical clustering model in Ref. [75)]. Then we compared these theoretical VF's with the observation of VF by Ref. [29)] for COBE normalized CDM and PIB models in §4.1. There we found that KSVF in the model LP – the spatially flat PIB model with $(\Omega_0,\ \lambda_0) = (0.2, 0.8)$ (Table I) – matches the observation best (Fig.1). We also discussed that the model LC – the CDM model with $(0.2, 0.8)$ – may become viable if the observed VF on galaxy scales is affected by the dissipative processes.

At first sight, one might expect that the inclusion of dark lenses and their evolution into GL statistics would lead to tighter limits on λ_0. However, when we compared the predictions of the theoretical VF's with the HST snapshot survey [30)] in §4.2, we saw that spatially flat models with non-zero Λ (model LC) are viable among the COBE normalized models (Fig.3). This is because the PSVF in low density universes underpredicts the number of galaxy scale lenses (Fig.1). Though the KSVF in the model LP is consistent with the VF observation, the model predicts higher lensing frequency at small separations than observed. We could find no COBE normalized cosmological model which satisfies both VF and GL observations, within the SIS, $\tilde{\alpha} = 1$ and no dust model.

In §5, we examined various uncertainties in the GL predictions systematically: the choice of the $\tilde{\alpha}$ parameter in the distance formula (Eq.[2·10]), core radius ξ_c, magnification bias, and the obscuration of images by dusts in the lensing galaxies. All these uncertainties reduce the GL prediction considerably from the standard calculation within a range of the realistic values of free parameters. The core radius and the dust obscuration are effective mainly at large and small separation range, respectively (Figs.5 and 7), while the uncertainties in $\tilde{\alpha}$ and the magnification bias reduce the GL prediction uniformly on all separation range. Because of these uncertainties, it is premature to put strong constraints on cosmological models, including Λ, from the rather small number of observed lensed sources. When a large number of QSO's are homogeneously sampled, a more reliable comparison will become possible. See Table II for a summary.

In §6, we made GL predictions relevant for the next generation survey like the SDSS. We believe that the predictions from theoretical VF will provide a promising test for Ω_0 and λ_0, combining with the COBE normalization. We proposed that the comparison between the predictions and the data should be made at large separation so that the various uncertainties do not enter: $\theta \gtrsim 7''$ may be ideal for cosmological tests because the theoretical VF is expected to be reliable on large scales. Lensing at the intermediate range ($3'' \lesssim \theta \lesssim 7''$) may provide information about the degree of dissipative effects on the galaxy formation. At the same time, the theory of VF needs improvements on the formation rate (§3.3) as well as on the dissipative effects.

Acknowledgements

We would like to thank K. Shimasaku and D. Maoz for providing the observational data, N. Sugiyama for permitting us to use his numerical program for the COBE normalization, and E.D. Stewart for careful reading of the manuscript. TTN would like to thank S. Sasaki, T. Kitayama and K. Ikumi for helpful discussions, and gratefully acknowledges the support from JSPS fellowship. This work is

supported in part by grants-in-aid by the Ministry of Education, Science, Sports and Culture of Japan (4125, 07CE2002).

Appendix A

—— Specific solutions of the Dyer-Roeder equation ——

In this appendix, the specific solutions of the Dyer-Roeder equation (Eq.[2·10]) are presented in the cases $\tilde{\alpha} = 1$ (filled beam) and $\tilde{\alpha} = 0$ (empty beam). We use the units $c = H_0 = 1$, and the notations $a := (1+z)^{-1}$ and

$$w := \Omega^{-1} - 1 = \begin{cases} w_0 a & (\lambda = 0) \\ w_0 a^3 & (\Omega + \lambda = 1) \end{cases} \tag{A·1}$$

with $w_0 := \Omega_0^{-1} - 1$ (see also Eq.[1·1]).
i) $\tilde{\alpha} = 1$ (filled beam)
i-i) $\lambda = 0$

$$D_1(z_1, z_2) = \frac{2a_2}{\sqrt{\Omega_0}} \left[a_1^{1/2}(1+w_1)^{1/2}(1+2w_2) - a_2^{1/2}(1+w_2)^{1/2}(1+2w_1) \right] \tag{A·2}$$

i-ii) $\Omega + \lambda = 1$

$$D_1(z_1, z_2) = \frac{2a_2}{\sqrt{\Omega_0}} \left[a_1^{1/2} F\left(\frac{1}{2}, \frac{1}{6}, \frac{7}{6}; -w_1\right) - a_2^{1/2} F\left(\frac{1}{2}, \frac{1}{6}, \frac{7}{6}; -w_2\right) \right], \tag{A·3}$$

where F is the hypergeometric function of type (2,1).
ii) $\tilde{\alpha} = 0$ (empty beam)
ii-i) $\lambda = 0$

$$\begin{aligned} D_0(z_1, z_2) = & \frac{1}{8\sqrt{\Omega_0} w_0^2 a_1} \Big[2a_1^{1/2}(1+w_1)^{1/2}(2w_1 - 3) \\ & - 2a_2^{1/2}(1+w_2)^{1/2}(2w_2 - 3) + 3|w_0|^{-1/2}(\eta_1 - \eta_2) \Big], \end{aligned} \tag{A·4}$$

where $\eta := \operatorname{arccosh}(1+2w)$ when $\Omega < 1$ and $\eta := \arccos(1+2w)$ when $\Omega > 1$.
ii-ii) $\Omega + \lambda = 1$

$$D_0(z_1, z_2) = \frac{2}{5\sqrt{\Omega_0} a_1} \left[a_1^{5/2} F\left(\frac{1}{2}, \frac{5}{6}, \frac{11}{6}; -w_1\right) - a_2^{5/2} F\left(\frac{1}{2}, \frac{5}{6}, \frac{11}{6}; -w_2\right) \right]. \tag{A·5}$$

We do not use Eqs.(A·3) and (A·5) because the evaluation of the hypergeometric function is much more time-consuming than the direct numerical integration of Eq.(2·10).

Appendix B

—— Analytic expressions for v_1 and v_2 ——

From Eqs.(2·6) and (2·16), v_1 and v_2 in Eqs.(2·13) and (2·15) are determined by the equation:

$$v^4 - X^2 v^{2p} - Y^2 = 0\,, \tag{B·1}$$

where

$$X := \frac{1}{4\pi} \frac{D_{\rm OS} \xi_{\rm c*}}{D_{\rm OL} D_{\rm LS}}\,, \quad Y := \frac{\theta}{8\pi} \frac{D_{\rm OS}}{D_{\rm LS}}\,. \tag{B·2}$$

The analytic expressions for v_1 and v_2 in the cases $p = 0, 1, 2, 3$ and 4 are:

$$p = 0 : \ v_1 = (X^2 + Y^2)^{1/4} \tag{B·3}$$

$$p = 1 : \ v_1 = [X^2 + (X^4 + 4Y^2)^{1/2}]^{1/2}/\sqrt{2} \tag{B·4}$$

$$p = 2 : \ v_1 = \sqrt{Y}(1 - X^2)^{-1/4} \tag{B·5}$$

$$p = 3 : \quad \begin{aligned} v_1 &= \frac{1}{X}\left[\frac{1}{3} + \frac{2}{3}\cos\left(\frac{2}{3}\pi - Z\right)\right]^{1/2}, \\ v_2 &= \frac{1}{X}\left[\frac{1}{3} + \frac{2}{3}\cos Z\right]^{1/2} \end{aligned} \tag{B·6}$$

$$p = 4 : \ v_{1,2} = (\sqrt{2}X)^{-1/2}[1 \mp (1 - 4X^2Y^2)^{1/2}]^{1/4}, \tag{B·7}$$

where

$$Z := \frac{1}{3}\arccos\left[1 - \frac{27}{2}(X^2Y)^2\right]. \tag{B·8}$$

When $p \leq 2$, $v_2 = \infty$.

Appendix C

—— *Spherical collapse in $\Omega + \lambda = 1$ universe* ——

Consider a local spherical region of radius r and mass M in an $\Omega + \lambda = 1$ universe with $\lambda > 0$. From the expansion equation:

$$\frac{d^2r}{dt^2} = -\frac{M}{r^2} + \frac{\Lambda}{3}r, \tag{C·1}$$

one obtains

$$t = \int_0^r dr' \left(2E + \frac{2M}{r'} + \frac{\Lambda}{3}r'^2\right)^{-1/2} \tag{C·2}$$

when $dr/dt > 0$ (we neglect the decaying mode). The sphere "turns around" at a radius $r_{\rm ta}$ defined by

$$E = -\frac{M}{r_{\rm ta}} - \frac{\Lambda}{6}r_{\rm ta}^2 \tag{C·3}$$

if

$$\zeta := \frac{\Lambda r_{\rm ta}^3}{6M} < \frac{1}{2} \tag{C·4}$$

[our ζ corresponds to $\eta/2$ of Ref. [114]]. Then Eq.(C·2) is rewritten as [115]

$$Ht = \left(\frac{\zeta}{\lambda}\right)^{1/2} \int_0^y dx \left[\frac{1}{x} - (1 + \zeta) + \zeta x^2\right]^{-1/2}, \tag{C·5}$$

where $y := r/r_{\rm ta}$. On the other hand, from Eq.(1·2) the age of the global universe in $\Omega + \lambda = 1$ models is

$$Ht = \frac{1}{3}(\Omega w)^{-1/2}\,{\rm arccosh}(1 + 2w), \tag{C·6}$$

where w is defined in Eq.(A·1). The sphere collapses to $r = 0$ in twice the turn-around time. In reality, however, it will reach a virialized state through the violent relaxation [116] and thereafter r stays constant $r_{\rm v}$ determined by [114]

$$4\zeta y_{\rm v}^3 - 2(1 + \zeta)y_{\rm v} + 1 = 0, \tag{C·7}$$

where and hereafter *the subscript* v *indicates the virialization time.* Eq.(C·7) has the solution

$$y_{\rm v} = \left(\frac{2+2\zeta}{3\zeta}\right)^{1/2} \cos\left\{\frac{2}{3}\pi - \frac{1}{3}\arccos\left[-\frac{1}{\zeta}\left(\frac{3\zeta}{2+2\zeta}\right)^{3/2}\right]\right\} \tag{C·8}$$

in the range $0 < \zeta < 0.5$. Let $\rho := 3M/(4\pi r^3)$ be the mean density inside the sphere. The overdensity against the background is written as

$$\vartheta := 1 + \delta := \frac{\rho}{\bar{\rho}} = \frac{w}{y^3\zeta}\,. \tag{C·9}$$

Let us calculate the overdensity of an virialized object at the virialization time:

$$\vartheta_{\rm v} := \frac{\rho_{\rm v}}{\bar{\rho}_{\rm v}} = \frac{w_{\rm v}}{y_{\rm v}^3\zeta}. \tag{C·10}$$

In order to relate ζ with $w_{\rm v}$, we equate the local time inside the sphere (Eq.[C·5]) with the global cosmic age (Eq.[C·6]) at the virialization epoch. The former is often approximated by the collapse time:

$$H_{\rm v}t_{\rm v} = 2\left(\frac{\zeta}{\lambda_{\rm v}}\right)^{1/2}\int_0^1 dx\left[\frac{1}{x} - (1+\zeta) + \zeta x^2\right]^{-1/2} \tag{C·11}$$

$$= \frac{1}{3}\lambda_{\rm v}^{-1/2}[AK(k) - B\Pi(\nu,k)]\,, \tag{C·12}$$

where $K(k)$ and $\Pi(\nu,k)$ are the complete elliptic integrals of the first and third kind, respectively (see Ref.[97] for their definitions), and

$$A := [1 + (1-2\zeta)^{1/2}]C, \quad B := 2(1-2\zeta)^{1/2}C, \tag{C·13}$$

$$C := 12\zeta^{-1/2}[2 - \zeta + 2(1-2\zeta)^{1/2}]^{-1/2} \tag{C·14}$$

$$k^2 := \frac{2 - \zeta - 2(1-2\zeta)^{1/2}}{2 - \zeta + 2(1-2\zeta)^{1/2}}\,, \tag{C·15}$$

$$\nu := -\zeta^{-2}[1 - \zeta - (1-2\zeta)^{1/2}]^2\,. \tag{C·16}$$

Note that Eq.(C·12) does not assume the spatial flatness $\Omega + \lambda = 1$. From Eqs.(C·6) and (C·12), ζ and $w_{\rm v}$ are related as

$$w_{\rm v} = \frac{1}{2}\{\cosh[AK(k) - B\Pi(\nu,k)] - 1\}\,. \tag{C·17}$$

Now we obtain the analytic formula for $\vartheta_{\rm v}$ in $\Omega + \lambda = 1$ universe through the parameter ζ. Given a value of ζ, one can compute $\vartheta_{\rm v}$ and $\Omega_{\rm v}$ from Eqs.(C·8), (C·10), (C·17) and (A·1). In practice, however, it is useful to write $\vartheta_{\rm v}$ as a function of $\Omega_{\rm v}$. For this purpose, we give the fitting formulae:

$$\vartheta_{\rm v} \simeq 18\pi^2\Omega_{\rm v}^{-0.573} \quad \text{or} \tag{C·18}$$

$$\vartheta_{\rm v} \simeq 18\pi^2(1 + 0.40929 w_{\rm v}^{0.90524}). \tag{C·19}$$

Eqs.(C·18) and (C·19) are accurate within 5% for $\Omega_{\rm v} > 0.1$ and 1.7% for $\Omega_{\rm v} > 0.01$, respectively.

Next, let us calculate $\delta_{\rm c}$, the density contrast in the early universe extrapolated linearly to the virialization time. Since $y \ll 1$ in the early stages, we expand the integrand of Eq.(C·5) in powers of x and keep the linear term only:

$$Ht = \left(\frac{\zeta}{\lambda}\right)^{1/2}\int_0^y \sqrt{x}[1 + \frac{1}{2}(1+\zeta)x]dx \tag{C·20}$$

$$= \frac{2}{3}\left(\frac{\zeta}{\lambda}\right)^{1/2} y^{3/2}[1 + \frac{3}{10}(1+\zeta)y]\,. \tag{C·21}$$

Similarly, $w \ll 1$ in Eq.(C·6) yields

$$Ht = \frac{2}{3}\Omega^{-1/2}\,. \tag{C·22}$$

Equating Eq.(C·21) with (C·22), y is written iteratively as

$$y = \left(\frac{w}{\zeta}\right)^{1/3}\left[1 - \frac{1}{5}(1+\zeta)\left(\frac{w}{\zeta}\right)^{1/3}\right]. \tag{C·23}$$

Substituting this into Eq.(C·9), the density contrast of the spherical region in the early universe is

$$\delta = \frac{3}{5}(1+\zeta)\left(\frac{w}{\zeta}\right)^{1/3} \tag{C·24}$$

which grows as $\propto w^{1/3} \propto a$ in accord with the linear perturbation theory [117]. The linear growth rate in $\Omega + \lambda = 1$ universe is [118]

$$D = w^{1/3} F\left(\frac{1}{3}, 1, \frac{11}{6}; -w\right) \tag{C·25}$$

which is normalized as $D/a \to w_0^{1/3}$ when $a \to 0$, with F being the hypergeometric function of type (2,1). Extrapolating Eq.(C·24) by Eq.(C·25) until $a_{\rm v}$, one obtains

$$\delta_{\rm c} = \frac{3}{5} F\left(\frac{1}{3}, 1, \frac{11}{6}; -w_{\rm v}\right)(1+\zeta)\left(\frac{w_{\rm v}}{\zeta}\right)^{1/3}. \tag{C·26}$$

One can compute $\delta_{\rm c}$ and $\Omega_{\rm v}$ from Eqs.(C·17), (C·26) and (A·1) through the parameter ζ. We give fitting formulae so that one can obtain $\delta_{\rm c}$ directly from a given value of $\Omega_{\rm v}$:

$$\delta_{\rm c} \simeq \frac{3}{20}(12\pi)^{2/3}\Omega_{\rm v}^{0.00539} \quad \text{or} \tag{C·27}$$

$$\delta_{\rm c} \simeq \frac{3}{20}(12\pi)^{2/3}(1 + 0.012299 \log_{10}\Omega_{\rm v}). \tag{C·28}$$

Eqs.(C·27) and (C·28) are accurate within 2.4% for $\Omega_{\rm v} > 0.1$ and 0.1% for $\Omega_{\rm v} > 0.01$, respectively.

Of more practical use (in, e.g., the PS theory) are the following quantities

$$\vartheta_{\rm v0} := \rho_{\rm v}/\bar{\rho}_0 = \vartheta_{\rm v}/a_{\rm v}^3 \tag{C·29}$$

$$\delta_{\rm c0} := \frac{D_0}{D_{\rm v}}\delta_{\rm c} = \frac{3}{5}F\left(\frac{1}{3}, 1, \frac{11}{6}; -w_0\right)(1+\zeta)\left(\frac{w_0}{\zeta}\right)^{1/3} \tag{C·30}$$

$$= \frac{3}{20}(12\pi)^{2/3}\frac{1}{a_{\rm v}}F\left(\frac{1}{3}, 1, \frac{11}{6}; -w_0\right)X(w_{\rm v})\,, \tag{C·31}$$

where

$$X(w_{\rm v}) \simeq \Omega_{\rm v}^{-0.215} \quad \text{or} \tag{C·32}$$

$$X(w_{\rm v}) \simeq 1 + (5.1066 w_{\rm v}^{-1.0812} + 2.0215 w_{\rm v}^{-0.35396})^{-1}. \tag{C·33}$$

The accuracies of Eqs.(C·32) and (C·33) are within 1.8% for $\Omega_{\rm v} > 0.1$ and 3.1% for $\Omega_{\rm v} > 0.01$, respectively. The corresponding formulae in an open ($\lambda = 0$) universe are found in Ref. [26].

References

[1] C. Alcock and N. Anderson, Astrophys. J. **302** (1986), 43.
[2] J.R. Gott III, M.G. Park and H.M. Lee, Astrophys. J. **344** (1989), 637.
[3] E.L. Turner, Astrophys. J. **365** (1990), L43.
[4] M. Fukugita, T. Futamase and M. Kasai, Mon. Not. R. Astron. Soc. **246** (1990), 25p.
[5] M. Fukugita and E.L. Turner, Mon. Not. R. Astron. Soc. **253** (1991), 99.
[6] M. Fukugita, T. Futamase, M. Kasai and E.L. Turner, Astrophys. J. **393** (1992), 3.
[7] D. Maoz and H.-W. Rix, Astrophys. J. **416** (1993), 425.
[8] C.S. Kochanek, Astrophys. J. **466** (1996), 638.
[9] G. Efstathiou, W.J. Sutherland and S.J. Maddox, Nature **348** (1990), 705.
[10] M. Fukugita, F. Takahara, K. Yamashita and Y. Yoshii, Astrophys. J. **361** (1990), L1.
[11] N.A. Bahcall and R. Cen, Astrophys. J. **398** (1992), L81.
[12] N.A. Bahcall and R. Cen, Astrophys. J. **407** (1993), L49.
[13] H. Ueda, M. Itoh, Y. Suto, Astrophys. J. **408** (1993), 3.
[14] N.A. Bahcall and S.P. Oh, Astrophys. J. **462** (1996), L49.
[15] Y. Suto, Prog. Theor. Phys. **90** (1993), 1173.
[16] A.R. Liddle, D.H. Lyth, P.T.P. Viana and M. White, Mon. Not. R. Astron. Soc. **282** (1996), 281.
[17] M.J. Pierce, et al., Nature **371** (1994), 385.
[18] W.L. Freedman, et al., Nature **371** (1994), 757.
[19] N.R. Tanvir, T. Shanks, H.C. Ferguson and D.R.T. Robinson, Nature **377** (1995), 27.
[20] B.C. Whitmore, W.B. Sparks, R.A. Lucas, F.D. Macchetto and J.A. Biretta, Astrophys. J. **454** (1995), L73.
[21] B. Chaboyer, Astrophys. J. **444** (1995), L9.
[22] J. Dunlop, et al., Nature **381** (1996), 581.
[23] T.T. Nakamura and Y. Suto, Astrophys. J. **447** (1995), L65.
[24] W.H. Press and P. Schechter, Astrophys. J. **187** (1974), 425.
[25] P.J.E. Peebles, Nature **327** (1987), 210.
[26] C. Lacey and S. Cole, Mon. Not. R. Astron. Soc. **262** (1993), 627.
[27] R. Narayan and S.D.M. White, Mon. Not. R. Astron. Soc. **231** (1988), 97p.
[28] C.S. Kochanek, Astrophys. J. **453** (1995), 545.
[29] K. Shimasaku, Astrophys. J. **413** (1993), 59.
[30] D. Maoz, et al., Astrophys. J. **409** (1993), 28.
[31] J. Ehlers and P. Schneider, Astron. Astrophys. **168** (1986), 57.
[32] G. Hinshaw and L.M. Krauss, Astrophys. J. **320** (1987), 468.
[33] M. Fukugita and P.J.E. Peebles, preprint, astro-ph/9305002.
[34] K. Tomita, in *Proceedings of Workshop on High-Redshift Objects and Gravitational Lens Effect* (Yukawa Institute for Theoretical Physics, Kyoto University, 1993), 35.
[35] S. Sasaki and F. Takahara, Mon. Not. R. Astron. Soc. **262** (1993), 681.
[36] T.T. Nakamura, Master Thesis, (University of Tokyo, 1996, unpublished).
[37] A. Kassiola and I. Kovner, Astrophys. J. **417** (1993), 450.
[38] R.D. Blandford and C.S. Kochanek, Astrophys. J. **321** (1987), 658.
[39] C.S. Kochanek and R.D. Blandford, Astrophys. J. **321** (1987), 676.
[40] J. Binney and S. Tremaine, *Galactic Dynamics* (Princeton University Press, Princeton, 1987).
[41] P. Schneider, J. Ehlers and E.E. Falco, *Gravitational Lenses* (Springer-Verlag, New York, 1992).
[42] T. Futamase, in *Relativistic Cosmology*, ed. M. Sasaki (Universal Academy Press, Tokyo, 1993).
[43] S. Seitz, P. Schneider and J. Ehlers, Class. Quamtum Grav. **11** (1994), 2345.
[44] T. Pyne and M. Birkinshaw, Astrophys. J. **458** (1996), 46.
[45] C.C. Dyer and R.C. Roeder, Astrophys. J. **174** (1972), L115.
[46] C.C. Dyer and R.C. Roeder, Astrophys. J. **180** (1973), L31.
[47] Ya.B. Zel'dovich, Sov. Astron. **8** (1964), 13; reprinted in *Selected Works of Yakov Borisovich Zeldovich, vol. 2*, eds. J.P. Ostriker, G.I. Barenblatt, R.A. Sunyaev (Princeton University Press, Princeton, 1993) 540.
[48] S. Weinberg, *Gravitation and Cosmology* (John Wiley & Sons, New York, 1972).
[49] J.E. Gunn, Astrophys. J. **150** (1967), 737.
[50] T. Futamase and M. Sasaki, Phys. Rev. **D40** (1989), 2502.
[51] K. Watanabe and M. Sasaki, Publ. Astron. Soc. Jpn. **42** (1990), L33.
[52] E.L. Turner, Astrophys. J. **242** (1980), L135.
[53] E.L. Turner, J.P. Ostriker and J.R. Gott III, Astrophys. J. **284** (1984), 1.
[54] P.J.E. Peebles, *Principles of Physical Cosmology* (Princeton University Press, Princeton, 1993).
[55] S. Weinberg, Astrophys. J. **208** (1976), L1.
[56] B.J. Boyle, T. Shanks and B.A. Peterson, Mon. Not. R. Astron. Soc. **235** (1988), 935.
[57] S. Wallington and R. Narayan, Astrophys. J. **403** (1993), 517.
[58] M. Bartelmann and P. Schneider, Astron. Astrophys. **239** (1990), 113.
[59] R.S. Ellis, M. Colles, T. Broadhurst, J. Heyl and K. Glazebrook, Mon. Not. R. Astron. Soc. **280** (1996), 235.
[60] R.O. Marzke, J.P. Huchra and M.J. Geller, Astrophys. J. **428** (1994), 43.

[61] S. Mao, Astrophys. J. **380** (1991), 9.
[62] S. Mao and C.S. Kochanek, Mon. Not. R. Astron. Soc. **268** (1994), 569.
[63] H.-W. Rix, D. Maoz, D., E.L. Turner and M. Fukugita, Astrophys. J. **435** (1994), 49.
[64] J.R. Gott III, Annu. Rev. Astron. Astrophys. **15** (1977), 235.
[65] R.A. Flores and J.R. Primack, Astrophys. J. **457** (1996), L5.
[66] K. Tomita, Publ. Astron. Soc. Jpn. **48** (1996), 265.
[67] T. Padmanabhan, *Structure formation in the universe* (Cambridge University Press, Cambridge, 1993).
[68] S. Cole and N. Kaiser, Mon. Not. R. Astron. Soc. **237** (1989), 1127.
[69] S.D.M. White and C.S. Frenk, Astrophys. J. **379** (1991), 52.
[70] J.R. Bond, S. Cole, G. Efstathiou and N. Kaiser, Astrophys. J. **379** (1991), 440.
[71] G. Efstathiou, C.S. Frenk, S.D.M. White and M. Davis, Mon. Not. R. Astron. Soc. **235** (1988), 715.
[72] C. Lacey and S. Cole, Mon. Not. R. Astron. Soc. **271** (1994), 676.
[73] S. Sasaki, Publ. Astron. Soc. Jpn. **46** (1994), 427.
[74] P.T.P. Viana and A.R. Liddle, Mon. Not. R. Astron. Soc. **281** (1996), 323.
[75] T. Kitayama and Y. Suto, Mon. Not. R. Astron. Soc. **280** (1996), 638.
[76] J.M. Bardeen, J.R. Bond, N. Kaiser and A.S. Szalay, Astrophys. J. **304** (1985), 15.
[77] W. Hu, E.F. Bunn and N. Sugiyama, Astrophys. J. **447** (1995), L59.
[78] N. Sugiyama, Astrophys. J. Suppl. **100** (1995), 281.
[79] C.J. Copi, D.N. Schramm and M.S. Turner, Science **267** (1995), 192.
[80] A.C. Edge, G.C. Stewart, A.C. Fabian and K.A. Arnaud, Mon. Not. R. Astron. Soc. **245** (1990), 559.
[81] N.A. Bahcall and L.M. Lubin, Astrophys. J. **426** (1994), 513.
[82] M.J. Rees and J.P. Ostriker, Mon. Not. R. Astron. Soc. **179** (1977), 541.
[83] S.D.M. White and M.J. Rees, Mon. Not. R. Astron. Soc. **183** (1978), 341.
[84] H.J. Mo and M. Fukugita, Astrophys. J. **467** (1996), L9.
[85] J.N. Bahcall, et al., Astrophys. J. **387** (1992), 56.
[86] D. Maoz, et al., Astrophys. J. **394** (1992), 54.
[87] D. Maoz, et al., Astrophys. J. **402** (1993), 69.
[88] D. Crampton, R.D. McClure and J.M Fletcher, Astrophys. J. **392** (1992), 23.
[89] J. Surdej, et al., Astron. J. **105** (1993), 2064.
[90] A.O. Jaunsen, M. Jablonski, B.R. Pettersen and R. Stabell, Astron. Astrophys. **300** (1995), 323.
[91] M. Schmidt and R.F. Green, Astrophys. J. **269** (1983), 352.
[92] D. Maoz, et al., Astrophys. J. **386** (1992), L1.
[93] P. Magain, J. Surdej, C. Vanderriest, B. Pirenne and D. Hutsemékers, Astron. Astrophys. **253** (1992), L13.
[94] P. Young, J.E. Gunn, J. Kristian, J.B. Oke, and J.A. Westphal, Astrophys. J. **244** (1981), 736.
[95] G. Meylan and S. Djorgovski, Astrophys. J. **338** (1989), L1.
[96] A.G. Michalitsianos, R.J. Oliversen and S.P. Maran, Astrophys. J. **458** (1996), 67.
[97] W.H. Press, S.A. Teukolsky, W.T. Vetterling and B.P. Flannery, *Numerical Recipes in Fortran* (Cambridge University Press, Cambridge, 1986).
[98] C.S. Kochanek, Astrophys. J. **419** (1993,12.
[99] W.H. Press and J.E. Gunn, Astrophys. J. **185** (1973), 397.
[100] M. Kasai, T. Futamase and F. Takahara, Phys. Lett. **A147** (1990), 97.
[101] M. Sasaki, Prog. Theor. Phys. **90** (1993), 753.
[102] T.R. Lauer, Astrophys. J. **292** (1985), 104.
[103] L.M. Krauss and M. White, Astrophys. J. **397** (1992), 357.
[104] R. Narayan and M. Bartelmann, *Lectures given at 13th Jerusalem Winter School in Theoretical Physics*, astro-ph/9606001.
[105] Y.-I. Byun et al., Astron. J. **111** (1996), 1889.
[106] K. Gebgardt et al., Astron. J. **112** (1996), 105.
[107] C.S. Kochanek, Astrophys. J. **436** (1994), 56.
[108] R. Cen, J.R. Gott III, J.P. Ostriker and E.L. Turner, Astrophys. J. **423** (1994), 1.
[109] C.S. Kochanek, Astrophys. J. **379** (1991), 517.
[110] M.J. Seaton, Mon. Not. R. Astron. Soc. **187** (1979), 73p.
[111] M.W. Wise and D.R. Silva, Astrophys. J. **461** (1996), 155.
[112] P. Goudfrooij, preprint, astro-ph/9601169.
[113] J.E. Gunn and D. Weinberg, in *Wide Field Spectroscopy and the Distant Universe*, eds. S.J. Maddox & A. Aragón-Salamanca (World Scientific, Singapore, 1995).
[114] O. Lahav, P.B. Lilje, J.R. Primack and M.J. Rees, Mon. Not. R. Astron. Soc. **251** (1991), 128.
[115] H. Hanami, Astrophys. J. **415** (1993), 42.
[116] D. Lynden-Bell, Mon. Not. R. Astron. Soc. **136** (1967), 101.
[117] P.J.E. Peebles, *The Large-Scale Structure of the Universe* (Princeton University Press, Princeton, 1980).
[118] T. Matsubara, PhD thesis, (Hiroshima University, 1995).